AIMS Mathematics, 11(2): 3394–3424.
DOI: 10.3934/math.2026138
Received: 22 November 2025
Revised: 16 January 2026
Accepted: 26 January 2026
Published: 04 February 2026

http://www.aimspress.com/journal/Math

Research article

A new analysis of isoparametric bilinear finite volume element scheme based on trapezoidal rule for anisotropic diffusion problems

Shengying Mu[1] **and Yanhui Zhou**[2,*]

[1] School of Mathematics and Statistics, Northeast Normal University, Changchun, 130024, China
[2] School of Mathematics and Systems Science, Guangdong Polytechnic Normal University, Guangzhou, 510665, China

* **Correspondence:** Email: zhouyh9@alumni.sysu.edu.cn.

Abstract: We studied the coercivity and error estimate of a modified isoparametric bilinear finite volume element scheme for anisotropic diffusion problems on quadrilateral meshes, where the scheme is obtained by employing the trapezoidal rule to approximate the line integrals in classical Q_1-finite volume element method. By an element analysis approach, we propose a new sufficient condition to ensure the coercivity result of the scheme, which is better than the existing results in [Q. Hong and J. Wu, *Adv. Comput. Math.*, **44** (2018), 897–922]. Under h^2-uniform quadrilateral mesh assumption, we prove the superconvergence $|u_I - u_h|_1 = O(h^2)$, where u_I is the isoparametric bilinear interpolation of exact solution u, and u_h is the finite volume element solution. As a result, an optimal L^2 error estimate of u_h is obtained. Some numerical experiments were carried out to verify the theoretical findings.

Keywords: isoparametric bilinear finite volume element scheme; coercivity; superconvergence; L^2 error estimate; anisotropic diffusion problem
Mathematics Subject Classification: 65N08, 65N12

1. Introduction

Since the finite volume element method (FVEM) presents local conservation property and other advantages, it has become one of the most popular numerical methods to solve partial differential equations. FVEM is also called a generalized difference method [22] or box method [1]. In the book [21] and review papers [24,44], the authors summarized the mathematical development of FVEM and presented some challenging research fronts. The FVEM has been applied to some challenging problems, e.g., eigenvalue problems [9], fractional equations [14, 19], adaptive algorithms [10], Cahn-Hilliard equation [36], nonlinear equations [5, 43], and Stokes problems [26, 38]. For general second-order elliptic equations, the element stiffness matrix of linear FVEM can be regarded as a

small perturbation of the corresponding linear finite element method on an arbitrary triangular mesh, leading to the coercivity result [2, 35]. As a result, the optimal H^1 error estimate can be proved by standard technique. Moreover, the optimal L^2 error estimate can be found in [11] for general triangular meshes. A theoretical analysis of higher-order FVEMs on triangular meshes can be found in [6,48,51] (coercivity) and [32,37] (L^2 error) for incomplete references.

However, the development of the classical isoparametric bilinear FVEM (Q_1-FVEM) on quadrilateral meshes has not proved satisfactory. To establish the coercivity result, most works require a quasi-parallelogram mesh assumption, see [23, 45]. Recently, for the coercivity of classical Q_1-FVEM, [18] proposed a sufficient condition that covers the traditional quasi-parallelogram mesh but, regrettably, not the arbitrary trapezoidal mesh. Under the coercivity result and quasi-parallelogram mesh assumption, by using Aubin-Nitsche technique, [27] proved the L^2 error estimate for a second-order elliptic equation with the anisotropic diffusion coefficient. By approximating the line integrals in classical Q_1-FVEM at the geometric center of the quadrilateral, [30] proposed a symmetric Q_1-FVE scheme, in which the global stiffness matrix was symmetric, and the error estimate was proved over a uniform rectangular mesh. [13, 17, 46] used trapezoidal, midpoint, and edge midpoint rules to approximate the line integrals, proposing some sufficient conditions to ensure the coercivity result of the new schemes; these conditions cover the traditional quasi-parallelogram but not the arbitrary trapezoidal mesh. Recently, by employing a linear combination of trapezoidal and midpoint quadrature rules (the weights depend on a parameter ω_K), [47] established the coercivity result of new schemes on the arbitrary trapezoidal and some general quadrilateral meshes. More studies of FVEM on quadrilateral meshes can be found in [28] (coercivity), [25,42] (L^2 error), and [16] (L^∞ error) for a non-exhaustive literature. Recently, the polygonal FVEMs were analyzed in [29] (monotone scheme), [40] (quadratic scheme), [41] (adaptive algorithm), and [49] (linear scheme).

Based on the coercivity result, one can study the superconvergence of the FVEM solution. On triangular meshes, by using the barycenters of triangles to construct the dual mesh, [15] proved that the difference between the linear FEM and FVEM solutions is of second order in energy norm. On a uniform rectangular mesh, and by Taylor expansion, [30] proved the L^2 error estimate and superconvergence. In 2012, on h^2-uniform quadrilateral mesh and by employing the geometric centers of quadrilaterals to construct the dual mesh, [27] showed that the error between the classical Q_1-FVEM solution and the interpolation of the exact solution is also of second order in energy norm. Further studies of superconvergence were presented in [33] (1D) and [4, 8, 31] (2D). However, the superconvergence of the modified isoparametric bilinear FVE scheme [17] has not been established. This work is motivated by the fact that, for the implementation of the program of classical Q_1-FVEM, the trapezoidal rule [17] is widely used to approximate the line integrals.

In this work, we intend to improve the coercivity and establish the superconvergence of the isoparametric bilinear FVE scheme constructed in [17]. First, unlike the coercivity analysis of [17] for a 4×4 matrix, here the element matrix is transformed into a 3×3 matrix, which enables us to suggest a new sufficient condition to guarantee the coercivity result. Moreover, it is interesting that this condition is better than that of [17], which is summarized in Theorem 3.2. Second, for the superconvergence, unlike [27], here the exact solution u and modified bilinear FVEM solution u_h are subjected to different variational forms. That is, u and u_h satisfy the continuous and discrete Petrov-Galerkin form, respectively; see Eqs (2.5) and (2.7). To obtain the superconvergence of the difference between u_I and u_h in energy norm, the bilinear form of the FVE scheme is decomposed into two parts.

The first part is the error between u and u_I; then, under the h^2-uniform quadrilateral mesh assumption and the superconvergence of bilinear interpolation on two adjacent quadrilateral elements, this error can be analyzed by some techniques. The second part is converted to the numerical integration about u, which can be analyzed on each quadrilateral element. Consequently, we reach the second-order superconvergence result. As a by-product, u_h converges to u with optimal convergence orders 1 and 2 under H^1 and L^2 norms, and the superconvergence results of u_h at geometric centers, interior vertices, and edge midpoints are all second order in an average gradient norm. In summary, the novelty of this paper is the improvement of the coercivity result of [17] and the establishment of the superconvergence.

The rest of this paper is organized as follows: In Section 2, we introduce the construction of the modified isoparametric bilinear finite volume element scheme for solving the anisotropic diffusion problems on quadrilateral meshes. A new coercivity result of the scheme is shown in Section 3. The superconvergence result and some corollaries are given in Section 4. Several numerical examples are presented in Section 5 to validate the theoretical findings, and in the last section, we provide a conclusion.

To avoid repetition, "$A \lesssim B$" indicates that A can be bounded by B multiplied by a constant irrelative to the parameters that A and B may depend on. Analogously, "$A \gtrsim B$" implies that B can be bounded by A, while "$A \sim B$" stands for both "$A \lesssim B$" and "$B \lesssim A$".

2. The Q_1-FVEM-TR scheme

We consider the following anisotropic diffusion problem

$$-\nabla \cdot (\Lambda \nabla u) = f, \text{ in } \Omega, \tag{2.1}$$

$$u = 0, \text{ on } \partial\Omega, \tag{2.2}$$

where $\Omega \subset \mathbb{R}^2$ is an open bounded connected polygonal domain, $f \in L^2(\Omega)$ is the source term, and the anisotropic diffusion coefficient $\Lambda(\boldsymbol{x})$ is a 2×2 symmetric and positive definite matrix; namely, there exist two positive constants $\underline{\lambda}$ and $\overline{\lambda}$ satisfying

$$\underline{\lambda}\|\boldsymbol{v}\|^2 \le \boldsymbol{v}^T \Lambda \boldsymbol{v} \le \overline{\lambda}\|\boldsymbol{v}\|^2, \quad \forall\, \boldsymbol{v} \in \mathbb{R}^2, \quad \forall\, \boldsymbol{x} = (x, y)^T \in \Omega,$$

and $\|\boldsymbol{v}\|$ is the Euclidean norm of vector $\boldsymbol{v}$. To simplify the statements of theoretical analysis, here we only consider the homogeneous Dirichlet boundary condition.

Suppose that the polygonal domain Ω is partitioned into a finite number of non-overlapped and strictly convex quadrilateral elements that form the so-called primary mesh $\mathcal{T}_h$, i.e., $\Omega = \cup\{K : K \in \mathcal{T}_h\}$ with $h = \max_{K\in\mathcal{T}_h} h_K$ being the mesh size and h_K the diameter of K. Moreover, $\mathcal{T}_h$ is assumed to conform in the sense that the intersection of any two different quadrilateral elements is a common edge, a common vertex, or empty. $\mathcal{T}_h$ is called regular provided that there exists a positive constant C_r independent of h, such that

$$\frac{h_K}{\rho_K} \le C_r, \quad \forall\, K \in \mathcal{T}_h, \tag{2.3}$$

where $\rho_K = \min_{1\le i\le 4}\{\text{diameter of the circle inscribed in } \triangle \boldsymbol{x}_{i-1}\boldsymbol{x}_i\boldsymbol{x}_{i+1}\}$; here and hereafter, i denotes, without special mention, a periodic index with period 4. Sometimes, we will use the quasi-regular assumption of the primary mesh, i.e., there exists a positive constant C_{qr} independent of h such that

$$|K| \ge C_{qr} h_K^2, \quad \forall\, K \in \mathcal{T}_h. \tag{2.4}$$

One can observe that Eq (2.3) yields Eq (2.4), but not vice versa (see Theorem 2.1 in [7]). Let $\mathcal{N}_K$, $\mathcal{E}_K$, and $\mathcal{M}_K$ be the set of four vertices $\boldsymbol{x}_i$, four edges $\boldsymbol{x}_i\boldsymbol{x}_{i+1}$, and four midpoints $\boldsymbol{y}_i$ of K, respectively. Then, we can denote $\mathcal{N}_h = \cup_{K\in\mathcal{T}_h}\mathcal{N}_K$, $\mathcal{E}_h = \cup_{K\in\mathcal{T}_h}\mathcal{E}_K$, $\mathcal{M}_h = \cup_{K\in\mathcal{T}_h}\mathcal{M}_K$, and $\mathcal{N}_h^\circ = \mathcal{N}_h\backslash\partial\Omega$, $\mathcal{E}_h^\circ = \mathcal{E}_h\backslash\partial\Omega$, $\mathcal{M}_h^\circ = \mathcal{M}_h\backslash\partial\Omega$ as the set of all vertices, edges, midpoints of edges and interior vertices, interior edges, and midpoints of interior edges of $\mathcal{T}_h$, respectively. Moreover, C_h is denoted as the set of all geometric centers of $\mathcal{T}_h$. Let the reference square element $\widehat{K} = \square\widehat{\boldsymbol{x}}_1\widehat{\boldsymbol{x}}_2\widehat{\boldsymbol{x}}_3\widehat{\boldsymbol{x}}_4 = [-1,1]^2$ on the (ξ,η) plane, where $\widehat{\boldsymbol{x}}_1 = (-1,-1)^T$, $\widehat{\boldsymbol{x}}_2 = (1,-1)^T$, $\widehat{\boldsymbol{x}}_3 = (1,1)^T$ and $\widehat{\boldsymbol{x}}_4 = (-1,1)^T$. For simplicity, here and hereafter, we will not distinguish between a point and its position vector: they share the same symbol. On $\widehat{K}$, one can introduce its four bilinear nodal basis functions as below

$$\widehat{\phi}_1 = \frac{(1-\xi)(1-\eta)}{4}, \quad \widehat{\phi}_2 = \frac{(1+\xi)(1-\eta)}{4}, \quad \widehat{\phi}_3 = \frac{(1+\xi)(1+\eta)}{4}, \quad \widehat{\phi}_4 = \frac{(1-\xi)(1+\eta)}{4},$$

which satisfy $\widehat{\phi}_i(\widehat{\boldsymbol{x}}_j) = \delta_{ij}$, where δ_{ij} is the Kronecker delta, namely $\delta_{ij} = 1$ if $i = j$, $\delta_{ij} = 0$ if $i \neq j$. For each strictly convex quadrilateral $K = \square\boldsymbol{x}_1\boldsymbol{x}_2\boldsymbol{x}_3\boldsymbol{x}_4$, there exists a unique invertible bilinear mapping $\mathcal{J}_K$ that maps $\widehat{K}$ onto K, satisfying $\mathcal{J}_K(\widehat{\boldsymbol{x}}_i) = \boldsymbol{x}_i$ $(i = 1,2,3,4)$; see Figure 1. It can be seen that the mapping $\mathcal{J}_K$ is given by

$$\mathcal{J}_K(\xi,\eta) = \boldsymbol{x}_K + \frac{1}{2}(\boldsymbol{m}_1\xi + \boldsymbol{m}_2\eta + \boldsymbol{m}_K\xi\eta),$$

where $\boldsymbol{x}_K$ is the geometric center of K, the vectors $\boldsymbol{m}_1$ and $\boldsymbol{m}_2$ (resp. $\boldsymbol{m}_K$) are related to the midpoints of opposite edges (resp. diagonals) of K, given by $\boldsymbol{x}_K = \sum_{i=1}^4 \boldsymbol{x}_i/4$, and

$$\boldsymbol{m}_1 = \frac{1}{2}(\boldsymbol{x}_2 + \boldsymbol{x}_3 - \boldsymbol{x}_1 - \boldsymbol{x}_4), \quad \boldsymbol{m}_2 = \frac{1}{2}(\boldsymbol{x}_3 + \boldsymbol{x}_4 - \boldsymbol{x}_1 - \boldsymbol{x}_2), \quad \boldsymbol{m}_K = \frac{1}{2}(\boldsymbol{x}_1 + \boldsymbol{x}_3 - \boldsymbol{x}_2 - \boldsymbol{x}_4).$$

With respect to the primary mesh $\mathcal{T}_h$, the trial function space U_h is defined as

$$U_h = \left\{u_h \in C(\overline{\Omega}) : u_h|_K = \widehat{u}_h \circ \mathcal{J}_K^{-1},\ \widehat{u}_h|_{\widehat{K}} \text{ is a bilinear function},\ \forall\, K \in \mathcal{T}_h,\ u_h|_{\partial\Omega} = 0\right\}.$$

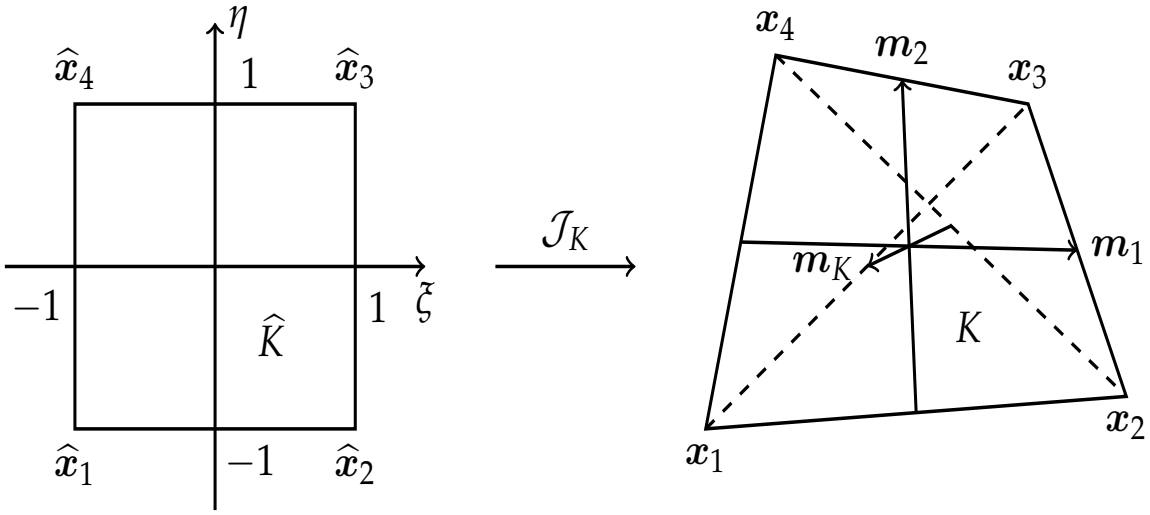

Figure 1. The bilinear mapping $\mathcal{J}_K$.

Next, we introduce the dual mesh. By connecting the geometric center $\boldsymbol{x}_K$ with its four edge midpoints $\boldsymbol{y}_i$, we partition K into four quadrilateral sub-elements. The contribution from K to the

control volume $\mathcal{D}_i$ is the quadrilateral $\mathcal{D}_{i,K} := \square \boldsymbol{x}_K \boldsymbol{y}_{i-1} \boldsymbol{x}_i \boldsymbol{y}_i$, and the whole control volume surrounding $\boldsymbol{x}_i$ is defined by $\mathcal{D}_i = \cup_{K \ni \boldsymbol{x}_i} \mathcal{D}_{i,K}$. The dual mesh $\mathcal{T}_h^*$ consists of all control volumes $\mathcal{T}_h^* = \{\mathcal{D}_i : \boldsymbol{x}_i \in \mathcal{N}_h\}$. In other words, all sub-elements sharing a common vertex of the primary mesh form a polygonal element of the dual mesh; see Figure 2 for an example. Based on the dual mesh $\mathcal{T}_h^*$, the *test function space* V_h is given by

$$V_h = \left\{ v_h \in L^2(\Omega) : v_h|_{\mathcal{D}_i} = \text{constant}, \ \forall\, \mathcal{D}_i \in \mathcal{T}_h^*, \ v_h|_{\partial\Omega} = 0 \right\}.$$

Then, we have $\dim U_h = \dim V_h$.

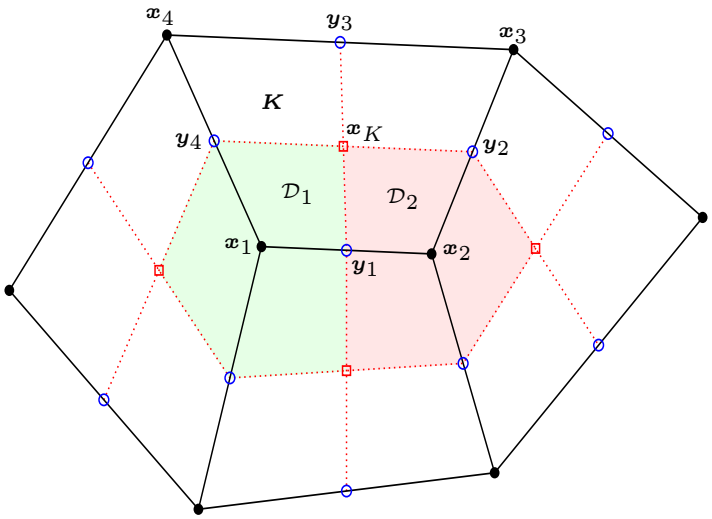

Figure 2. The primary mesh $\mathcal{T}_h$ (solid lines) and its associated dual mesh $\mathcal{T}_h^*$ (dotted lines).

By using the Green's formula, we deduce from Eq (2.1) that

$$-\int_{\partial\mathcal{D}_i} (\Lambda \nabla u) \cdot \boldsymbol{n}_i^* \, \mathrm{d}s = \int_{\mathcal{D}_i} f \, \mathrm{d}x\mathrm{d}y, \quad \forall\, \boldsymbol{x}_i \in \mathcal{N}_h^\circ,$$

where $\boldsymbol{n}_i^*$ is the unit outward normal vector along the boundary of $\mathcal{D}_i$. Rearranging the above equation, it is equivalent to

$$a_h(u, v_h) = (f, v_h), \quad \forall\, v_h \in V_h, \tag{2.5}$$

where

$$a_h(u, v_h) = \sum_{\boldsymbol{x}_i \in \mathcal{N}_h^\circ} v_i \int_{\partial\mathcal{D}_i} (-\Lambda \nabla u) \cdot \boldsymbol{n}_i^* \, \mathrm{d}s, \quad (f, v_h) = \sum_{\boldsymbol{x}_i \in \mathcal{N}_h^\circ} v_i \int_{\mathcal{D}_i} f \, \mathrm{d}x\mathrm{d}y$$

and $v_i = v_h(\boldsymbol{x}_i)$. In Eq (2.5), replacing u by u_h, one can reach the classical Q_1-FVEM to solve Eqs (2.1) and (2.2), i.e., find $u_h \in U_h$ such that

$$a_h(u_h, v_h) = (f, v_h), \quad \forall\, v_h \in V_h.$$

Note that $v_i = 0$ provided that $\boldsymbol{x}_i \in \partial\Omega$, then rewrite the bilinear form of $a_h(\cdot, \cdot)$, we obtain

$$a_h(u_h, v_h) = \sum_{K \in \mathcal{T}_h} a_{K,h}(u_h, v_h), \quad a_{K,h}(u_h, v_h) = \sum_{i=1}^{4} [v_h]_{\boldsymbol{x}_K \boldsymbol{y}_i} \int_{\boldsymbol{x}_K \boldsymbol{y}_i} (-\Lambda \nabla u_h) \cdot \boldsymbol{n}_{K,i}^* \, \mathrm{d}s, \tag{2.6}$$

where $[v_h]_{\boldsymbol{x}_K\boldsymbol{y}_i} = v_{i+1} - v_i$ is the jump across $\boldsymbol{x}_K\boldsymbol{y}_i$ and

$$\boldsymbol{n}^*_{K,i} = \frac{1}{\|\boldsymbol{y}_i - \boldsymbol{x}_K\|}\mathcal{R}(\boldsymbol{y}_i - \boldsymbol{x}_K), \quad \mathcal{R} = \begin{pmatrix} 0 & 1 \\ -1 & 0 \end{pmatrix}.$$

By employing the trapezoidal rule to approximate the line integrals in Eq (2.6),

$$\int_{\boldsymbol{x}_K\boldsymbol{y}_i} (-\Lambda\nabla u_h)\cdot \boldsymbol{n}^*_{K,i}\,\mathrm{d}s \approx \frac{1}{2}(\boldsymbol{x}_K - \boldsymbol{y}_i)^T\mathcal{R}^T\Lambda_K\left[\nabla u_h(\boldsymbol{x}_K) + \nabla u_h(\boldsymbol{y}_i)\right],$$

where Λ_K denotes the constant restriction of Λ on K (e.g., $\Lambda_K = \Lambda(\boldsymbol{x}_K)$), and we reach the so-called Q_1-FVEM-TR scheme, given by

$$\widetilde{a}_h(u_h, v_h) = (f, v_h), \quad \forall\, v_h \in V_h, \tag{2.7}$$

where

$$\widetilde{a}_h(u_h, v_h) = \sum_{K\in\mathcal{T}_h} \widetilde{a}_{K,h}(u_h, v_h), \tag{2.8}$$

$$\widetilde{a}_{K,h}(u_h, v_h) = \frac{1}{2}\sum_{i=1}^{4}[v_h]_{\boldsymbol{x}_K\boldsymbol{y}_i}(\boldsymbol{x}_K - \boldsymbol{y}_i)^T\mathcal{R}^T\Lambda_K\left[\nabla u_h(\boldsymbol{x}_K) + \nabla u_h(\boldsymbol{y}_i)\right].$$

We mention that the Q_1-FVEM-TR scheme (2.7) is constructed in [17]. For any $u_h \in U_h$, we have $u_h = \sum_{i=1}^4 u_i\widehat{\phi}_i$ in each $K \in \mathcal{T}_h$. Let

$$\boldsymbol{\psi}_1(\xi,\eta) = \frac{1}{4}\mathbb{J}_K^{-1}(\xi,\eta)\begin{pmatrix} 1-\eta \\ 0 \end{pmatrix}, \quad \boldsymbol{\psi}_2(\xi,\eta) = \frac{1}{4}\mathbb{J}_K^{-1}(\xi,\eta)\begin{pmatrix} 0 \\ 1+\xi \end{pmatrix},$$
$$\boldsymbol{\psi}_3(\xi,\eta) = -\frac{1}{4}\mathbb{J}_K^{-1}(\xi,\eta)\begin{pmatrix} 1+\eta \\ 0 \end{pmatrix}, \quad \boldsymbol{\psi}_4(\xi,\eta) = \frac{1}{4}\mathbb{J}_K^{-1}(\xi,\eta)\begin{pmatrix} 0 \\ \xi-1 \end{pmatrix}.$$

It follows that

$$\nabla u_h = \mathbb{J}_K^{-1}(\xi,\eta)\sum_{i=1}^{4} u_i\widehat{\nabla\phi}_i = \sum_{i=1}^{4}(u_{i+1} - u_i)\boldsymbol{\psi}_i(\xi,\eta),$$

where $\widehat{\nabla} = (\partial/\partial\xi, \partial/\partial\eta)^T$ and we have used the fact $\mathbb{J}_K^{-1}(\xi,\eta)\widehat{\nabla\phi}_i = \boldsymbol{\psi}_{i-1} - \boldsymbol{\psi}_i$. Let Π_h^* be a linear mapping that maps $u_h \in U_h$ to $u_h^* := \Pi_h^* u_h \in V_h$ satisfying $u_h^*(\boldsymbol{x}) = u_h(\boldsymbol{x})$, $\forall\, \boldsymbol{x} \in \mathcal{N}_h^\circ$. By denoting $\delta\boldsymbol{U}_K = (u_2 - u_1, u_3 - u_2, u_4 - u_3, u_1 - u_4)^T$ and $\widehat{\boldsymbol{x}} = (\xi,\eta)^T = \mathcal{J}_K^{-1}(\boldsymbol{x})$, we have

$$\widetilde{a}_{K,h}(u_h, u_h^*) = \delta\boldsymbol{U}_K^T\mathbb{A}_K\delta\boldsymbol{U}_K, \tag{2.9}$$

where

$$\mathbb{A}_K = \left(a_{K,ij}\right)_{4\times 4}, \quad a_{K,ij} = \frac{1}{2}(\boldsymbol{x}_K - \boldsymbol{y}_i)^T\mathcal{R}^T\Lambda_K\left[\boldsymbol{\psi}_j(\widehat{\boldsymbol{x}}_K) + \boldsymbol{\psi}_j(\widehat{\boldsymbol{y}_i})\right]. \tag{2.10}$$

By transforming $\mathbb{A}_K$ to a 3×3 matrix, in the next section we give a new sufficient condition to ensure the coercivity result.

3. New coercivity result

For convenience of exposition, we define the following notations

$$\overline{\beta}_K = \frac{\boldsymbol{m}_1 \cdot (\mathcal{R}\boldsymbol{m}_K)}{|K|}, \quad \overline{\gamma}_K = \frac{\boldsymbol{m}_K \cdot (\mathcal{R}\boldsymbol{m}_2)}{|K|}, \quad m_{ij} = \frac{1}{4|K|} (\mathcal{R}\boldsymbol{m}_i)^T \Lambda_K \left(\mathcal{R}\boldsymbol{m}_j\right), \tag{3.1}$$

$$\mu_1 = \mu_2 + \mu_3, \quad \mu_2 = \frac{2m_{11}}{1-\overline{\beta}_K^2}, \quad \mu_3 = \frac{2m_{22}}{1-\overline{\gamma}_K^2}, \tag{3.2}$$

$$\zeta_1 = m_{11} - \frac{\mu_3^2}{16\mu_1}\overline{\beta}_K^2, \quad \zeta_2 = m_{22} - \frac{\mu_2^2}{16\mu_1}\overline{\gamma}_K^2, \quad \zeta_3 = m_{12} + \frac{\mu_2\mu_3}{16\mu_1}\overline{\beta}_K\overline{\gamma}_K. \tag{3.3}$$

To present the coercivity result, we introduce the following assumption:
(**A1**) There exists a positive constant ϱ, independent of K and h, such that $\zeta_1\zeta_2 - \zeta_3^2 \geq \varrho$.

Theorem 3.1. *Assume that $\mathcal{T}_h$ consists of strictly convex quadrilaterals, under the assumptions* (2.3) *and* (**A1**)*, we have*

$$\widetilde{a}_h(u_h, u_h^*) \gtrsim |u_h|_1^2, \quad \forall\, u_h \in U_h, \tag{3.4}$$

where the hidden constant is independent of h, and $|\cdot|_1$ denotes the standard H^1 semi-norm.

To prove the new coercivity result (3.4), we first present some lemmas.

Lemma 3.1. *Assume that K is a strictly convex quadrilateral, then we have*

$$\left|\overline{\beta}_K\right| + \left|\overline{\gamma}_K\right| < 1, \quad \boldsymbol{m}_K = \overline{\gamma}_K\boldsymbol{m}_1 + \overline{\beta}_K\boldsymbol{m}_2. \tag{3.5}$$

For the m_{ij} defined by Eq (3.1)*, we have*

$$m_{12} = m_{21}, \quad m_{11}m_{22} - m_{12}^2 = \frac{1}{16}\det(\Lambda_K). \tag{3.6}$$

Moreover, under the geometric assumption (2.4)

$$|m_{12}| < \frac{\overline{\lambda}}{4C_{qr}}, \quad \frac{C_{qr}\underline{\lambda}}{4} < m_{ii} < \frac{\overline{\lambda}}{4C_{qr}}, \quad i = 1, 2.$$

Proof. The proof of this lemma can be found in some papers, e.g., Lemmas 1 and 2 of [18], or Lemmas 1 and 2 of [47]. □

Lemma 3.2. *For the ζ_1 and ζ_2 defined in Eq* (3.3)*, we have $4\zeta_1 + \zeta_2 > 0$.*

Proof. Noticing $\mu_i > 0\,(i = 1, 2, 3)$, and Eqs (3.2) and (3.5), it holds that

$$4\zeta_1 + \zeta_2 \geq 4m_{11} - \frac{\mu_3}{4}\overline{\beta}_K^2 + m_{22} - \frac{\mu_2}{16}\overline{\gamma}_K^2 > 4m_{11} + m_{22} - \frac{\mu_3}{4}\left(1-\overline{\gamma}_K^2\right) - \frac{\mu_2}{16}\left(1-\overline{\beta}_K^2\right) = \frac{1}{8}(31m_{11} + 4m_{22}),$$

leads to the desired result. □

Lemma 3.3. *For the $\mathbb{A}_K$ defined by Eq* (2.10)*, we have*

$$\mathbb{A}_K = \begin{pmatrix} \frac{3-\overline{\gamma}_K}{2(1-\overline{\gamma}_K)}m_{22} & \frac{\overline{\beta}_K m_{22}}{2(1-\overline{\gamma}_K)} - m_{12} & -\frac{m_{22}}{2} & m_{12} - \frac{\overline{\beta}_K m_{22}}{2(1-\overline{\gamma}_K)} \\ -\frac{\overline{\gamma}_K m_{11}}{2(1+\overline{\beta}_K)} - m_{12} & \frac{3+\overline{\beta}_K}{2(1+\overline{\beta}_K)}m_{11} & \frac{\overline{\gamma}_K m_{11}}{2(1+\overline{\beta}_K)} + m_{12} & -\frac{m_{11}}{2} \\ -\frac{m_{22}}{2} & \frac{\overline{\beta}_K m_{22}}{2(1+\overline{\gamma}_K)} + m_{12} & \frac{3+\overline{\gamma}_K}{2(1+\overline{\gamma}_K)}m_{22} & -\frac{\overline{\beta}_K m_{22}}{2(1+\overline{\gamma}_K)} - m_{12} \\ m_{12} - \frac{\overline{\gamma}_K m_{11}}{2(1-\overline{\beta}_K)} & -\frac{m_{11}}{2} & \frac{\overline{\gamma}_K m_{11}}{2(1-\overline{\beta}_K)} - m_{12} & \frac{3-\overline{\beta}_K}{2(1-\overline{\beta}_K)}m_{11} \end{pmatrix}.$$

Proof. A direct calculation yields that $\boldsymbol{x}_K - \boldsymbol{y}_1 = \boldsymbol{y}_3 - \boldsymbol{x}_K = \boldsymbol{m}_2/2$, $\boldsymbol{x}_K - \boldsymbol{y}_4 = \boldsymbol{y}_2 - \boldsymbol{x}_K = \boldsymbol{m}_1/2$ and

$$\mathbb{J}_K^{-1}(\xi,\eta) = \frac{2}{|K|\left(1+\overline{\beta}_K\xi+\overline{\gamma}_K\eta\right)}\left[\mathcal{R}(\boldsymbol{m}_2+\xi\boldsymbol{m}_K), -\mathcal{R}(\boldsymbol{m}_1+\eta\boldsymbol{m}_K)\right].$$

It follows that

$$\boldsymbol{\psi}_1(\widehat{\boldsymbol{x}}_K) = \frac{1}{2|K|}\mathcal{R}\boldsymbol{m}_2, \quad \boldsymbol{\psi}_1(\widehat{\boldsymbol{y}}_1) = \frac{1}{(1-\overline{\gamma}_K)|K|}\mathcal{R}\boldsymbol{m}_2,$$

implying that

$$a_{K,11} = \frac{3-\overline{\gamma}_K}{2(1-\overline{\gamma}_K)}m_{22}.$$

Similarly, we obtain the remaining entries of $\mathbb{A}_K$ and complete the proof. □

Let $\delta\boldsymbol{V}_K = (u_2-u_1, u_3-u_2, u_4-u_3)^T$ and

$$\mathbb{P} = \begin{pmatrix} 1 & 0 & 0 \\ 0 & 1 & 0 \\ 0 & 0 & 1 \\ -1 & -1 & -1 \end{pmatrix},$$

then we have $\delta\boldsymbol{U}_K = \mathbb{P}\delta\boldsymbol{V}_K$. Denote $\mathbb{B}_K \triangleq \mathbb{P}^T\mathbb{A}_K\mathbb{P} = \sum_{i=1}^3 \mathbb{B}_{K,i}$, where

$$\mathbb{B}_{K,1} = \frac{m_{11}}{1-\overline{\beta}_K}\begin{pmatrix} \frac{1}{2}\left(3-\overline{\beta}_K+\overline{\gamma}_K\right) & 2-\overline{\beta}_K & \frac{1}{2}\left(3-\overline{\beta}_K-\overline{\gamma}_K\right) \\ \frac{2+\overline{\beta}_K-\overline{\beta}_K^2+\overline{\beta}_K\overline{\gamma}_K}{1+\overline{\beta}_K} & \frac{4-2\overline{\beta}_K^2}{1+\overline{\beta}_K} & \frac{2+\overline{\beta}_K-\overline{\beta}_K^2-\overline{\beta}_K\overline{\gamma}_K}{1+\overline{\beta}_K} \\ \frac{1}{2}\left(3-\overline{\beta}_K+\overline{\gamma}_K\right) & 2-\overline{\beta}_K & \frac{1}{2}\left(3-\overline{\beta}_K-\overline{\gamma}_K\right) \end{pmatrix},$$

$$\mathbb{B}_{K,2} = m_{22}\begin{pmatrix} \frac{3+\overline{\beta}_K-\overline{\gamma}_K}{2(1-\overline{\gamma}_K)} & \frac{\overline{\beta}_K}{1-\overline{\gamma}_K} & \frac{\overline{\beta}_K+\overline{\gamma}_K-1}{2(1-\overline{\gamma}_K)} \\ 0 & 0 & 0 \\ \frac{\overline{\beta}_K-\overline{\gamma}_K-1}{2(1+\overline{\gamma}_K)} & \frac{\overline{\beta}_K}{1+\overline{\gamma}_K} & \frac{3+\overline{\beta}_K+\overline{\gamma}_K}{2(1+\overline{\gamma}_K)} \end{pmatrix}, \quad \mathbb{B}_{K,3} = 2m_{12}\begin{pmatrix} -1 & -1 & 0 \\ -1 & 0 & 1 \\ 0 & 1 & 1 \end{pmatrix}.$$

Lemma 3.4. *Let $\mathbb{B}_K^S = (\mathbb{B}_K + \mathbb{B}_K^T)/2$ be the symmetric part of $\mathbb{B}_K$ and $\mathbb{T} = \Pi_{i=1}^4 \mathbb{T}_i$, where*

$$\mathbb{T}_1 = \begin{pmatrix} 1 & 0 & 0 \\ -1 & 1 & -\frac{1}{2} \\ 1 & 0 & 1 \end{pmatrix}, \quad \mathbb{T}_2 = \begin{pmatrix} 1 & 0 & \frac{\overline{\gamma}_K - 2}{4} \\ 0 & 1 & 0 \\ 0 & 0 & 1 \end{pmatrix}, \quad \mathbb{T}_3 = \begin{pmatrix} 1 & -\frac{\mu_1+\mu_2}{2\mu_1}\overline{\beta}_K & 0 \\ 0 & 1 & 0 \\ 0 & 0 & 1 \end{pmatrix}, \quad \mathbb{T}_4 = \begin{pmatrix} 1 & 0 & \frac{\mu_3}{4\mu_1}\overline{\gamma}_K \\ 0 & 1 & 0 \\ 0 & 0 & 1 \end{pmatrix}.$$

Then, we have

$$\mathbb{T}^T \mathbb{B}_K^S \mathbb{T} = \begin{pmatrix} \mu_1 & 0 & 0 \\ 0 & 4\zeta_1 & 2\zeta_3 \\ 0 & 2\zeta_3 & \zeta_2 \end{pmatrix}. \tag{3.7}$$

As a result, $\mathbb{B}_K^S$ is positive definite if and only if $\zeta_1\zeta_2 - \zeta_3^2 > 0$.

Proof. Based on the definition of $\mathbb{T}_i\,(i = 1, 2, 3, 4)$, we reach Eq (3.7) by some straightforward calculations. Since $\mu_1 > 0$, we find that $\mathbb{B}_K^S$ is positive definite if and only if the characteristic equation $\lambda^2 - (4\zeta_1 + \zeta_2)\lambda + 4(\zeta_1\zeta_2 - \zeta_3^2) = 0$ has positive roots. Recalling Lemma 3.2, we conclude that $\mathbb{B}_K^S$ is positive definite if and only if $\zeta_1\zeta_2 - \zeta_3^2 > 0$. □

Lemma 3.5. *For the matrix $\mathbb{T}$ defined in Lemma 3.4, we have $\|\mathbb{T}\| < 14$, where $\|\cdot\|$ denotes the spectral norm of the matrix.*

Proof. Noticing that $\|\mathbb{T}_i\|$ equals to the square root of the maximal eigenvalue of $\mathbb{T}_i^T\mathbb{T}_i$, then by some direct computations, we obtain

$$\|\mathbb{T}_i\| = \sqrt{\frac{t_i^2 + 2 + \sqrt{\left(t_i^2+2\right)^2 - 4}}{2}} < \sqrt{t_i^2 + 2}, \quad i = 2, 3, 4,$$

where

$$t_2 = \frac{\overline{\gamma}_K - 2}{4}, \quad t_3 = -\frac{\mu_1 + \mu_2}{2\mu_1}\overline{\beta}_K, \quad t_4 = \frac{\mu_3}{4\mu_1}\overline{\gamma}_K.$$

Recalling Eq (3.5), we find that

$$\|\mathbb{T}_2\| < \frac{\sqrt{41}}{4}, \quad \|\mathbb{T}_3\| < \sqrt{3}, \quad \|\mathbb{T}_4\| < \frac{\sqrt{33}}{4}.$$

It can be checked that $\mathbb{T}_1 = \mathbb{T}_{11}\mathbb{T}_{12}\mathbb{T}_{13}$, where

$$\mathbb{T}_{11} = \begin{pmatrix} 1 & 0 & 0 \\ -1 & 1 & 0 \\ 0 & 0 & 1 \end{pmatrix}, \quad \mathbb{T}_{12} = \begin{pmatrix} 1 & 0 & 0 \\ 0 & 1 & 0 \\ 1 & 0 & 1 \end{pmatrix}, \quad \mathbb{T}_{13} = \begin{pmatrix} 1 & 0 & 0 \\ 0 & 1 & -\frac{1}{2} \\ 0 & 0 & 1 \end{pmatrix}.$$

It holds that

$$\|\mathbb{T}_{11}\| = \|\mathbb{T}_{12}\| = \sqrt{\frac{3 + \sqrt{5}}{2}}, \quad \|\mathbb{T}_{13}\| = \sqrt{\frac{9 + \sqrt{17}}{8}}.$$

Finally, we complete the proof by noticing $\|\mathbb{T}\| \le (\Pi_{i=1}^3 \|\mathbb{T}_{1i}\|)(\Pi_{j=2}^4 \|\mathbb{T}_j\|)$. □

Lemma 3.6. *Under the assumptions* (2.4) *and* (**A1**)*, we have*

$$\boldsymbol{v}^T\mathbb{B}_K\boldsymbol{v} \geq \frac{C_{qr}\varrho}{98\overline{\lambda}}\|\boldsymbol{v}\|^2, \quad \forall\, \boldsymbol{v} \in \mathbb{R}^3. \tag{3.8}$$

Proof. It follows from Eq (3.7) that

$$\boldsymbol{v}^T\mathbb{B}_K\boldsymbol{v} = \left(\mathbb{T}^{-1}\boldsymbol{v}\right)^T\left(\mathbb{T}^T\mathbb{B}_K^S\mathbb{T}\right)\left(\mathbb{T}^{-1}\boldsymbol{v}\right) \geq c_K\|\mathbb{T}^{-1}\boldsymbol{v}\|^2,$$

where $c_K = \min\{\mu_1, \lambda_K\}$ and λ_K is the minimal root of $\lambda^2 - (4\zeta_1 + \zeta_2)\lambda + 4(\zeta_1\zeta_2 - \zeta_3^2) = 0$, i.e.,

$$\lambda_K = \frac{1}{2}\left[4\zeta_1 + \zeta_2 - \sqrt{(4\zeta_1 + \zeta_2)^2 - 16\left(\zeta_1\zeta_2 - \zeta_3^2\right)}\right] \leq \frac{4\zeta_1 + \zeta_2}{2} \leq \frac{4m_{11} + m_{22}}{2}.$$

By Eq (3.5), we have $\mu_2 \geq 2m_{11}$ and $\mu_3 \geq 2m_{22}$, leading to $\mu_1 \geq 2m_{11} + 2m_{22}$ and

$$c_K = \lambda_K = \frac{8\left(\zeta_1\zeta_2 - \zeta_3^2\right)}{4\zeta_1 + \zeta_2 + \sqrt{(4\zeta_1 + \zeta_2)^2 - 16\left(\zeta_1\zeta_2 - \zeta_3^2\right)}} \geq \frac{4\left(\zeta_1\zeta_2 - \zeta_3^2\right)}{4\zeta_1 + \zeta_2} \geq \frac{\zeta_1\zeta_2 - \zeta_3^2}{m_{11} + m_{22}} \geq \frac{2C_{qr}\varrho}{\overline{\lambda}}.$$

Noting Lemma 3.5,

$$\|\mathbb{T}^{-1}\boldsymbol{v}\| \geq \frac{1}{\|\mathbb{T}\|}\|\boldsymbol{v}\| \geq \frac{1}{14}\|\boldsymbol{v}\|,$$

and then we reach Eq (3.8). □

Lemma 3.7. *If Eq* (2.3) *holds, then for any $u_h \in U_h$, we have $|u_h|_{1,K} \sim \|\delta\boldsymbol{U}_K\|$.*

Proof. The proof can be found in Proposition 1 of [23]. □

The proof of Theorem 3.1. By Eqs (2.8), (2.9), and (3.8), we deduce that

$$\widetilde{a}_h\left(u_h, u_h^*\right) = \sum_{K\in\mathcal{T}_h}\delta\boldsymbol{U}_K^T\mathbb{A}_K\delta\boldsymbol{U}_K = \sum_{K\in\mathcal{T}_h}\delta\boldsymbol{V}_K^T\mathbb{B}_K\delta\boldsymbol{V}_K \geq \frac{C_{qr}\varrho}{98\overline{\lambda}}\sum_{K\in\mathcal{T}_h}\|\delta\boldsymbol{V}_K\|^2.$$

Thus, by recalling Lemma 3.7 and the fact that $\|\delta\boldsymbol{U}_K\| \sim \|\delta\boldsymbol{V}_K\|$, we get Eq (3.4). □

Next, we discuss the relation of coercivity results between this work and [17]. The following Theorem 3.2 indicates that (**A1**) is weaker than that of (**H1**) in [17]. As a comparison, by using the notations of this work, (**H1**) in [17] can be rewritten as follows:

(**H1**) There exists a positive constant ϱ^{HW}, independent of K and h, such that

$$\zeta_1^{HW}\zeta_2^{HW} - m_{12}^2 \geq \varrho^{HW},$$

where

$$\zeta_1^{HW} = m_{22} - \frac{\mu_2}{16}\overline{\gamma}_K^2, \quad \zeta_2^{HW} = m_{11} - \frac{\mu_3}{16}\overline{\beta}_K^2.$$

Theorem 3.2. *Assume that $\mathcal{T}_h$ consists of strictly convex quadrilaterals, then the condition* (**H1**) *of [17] implies* (**A1**)*, but not vice versa.*

Proof. A direct calculation yields that

$$\left(\zeta_1\zeta_2-\zeta_3^2\right)-\left(\zeta_1^{HW}\zeta_2^{HW}-m_{12}^2\right)=\frac{\mu_2\mu_3}{256\mu_1}\left(16\overline{\gamma}_K^2m_{11}+16\overline{\beta}_K^2m_{22}-32\overline{\beta}_K\overline{\gamma}_Km_{12}-\mu_1\overline{\beta}_K^2\overline{\gamma}_K^2\right).$$

If (**H1**) holds, then by noticing Eq (32) of [17], we have $\zeta_i^{HW}>0\,(i=1,2)$. As a result

$$\begin{aligned}16\overline{\gamma}_K^2m_{11}+16\overline{\beta}_K^2m_{22}&=\left(16\overline{\gamma}_K^2\zeta_2^{HW}+\mu_3\overline{\beta}_K^2\overline{\gamma}_K^2\right)+\left(16\overline{\beta}_K^2\zeta_1^{HW}+\mu_2\overline{\beta}_K^2\overline{\gamma}_K^2\right)\\&\geq 32\left|\overline{\beta}_K\overline{\gamma}_K\sqrt{\zeta_1^{HW}\zeta_2^{HW}}\right|+\mu_1\overline{\beta}_K^2\overline{\gamma}_K^2\\&\geq 32\left|\overline{\beta}_K\overline{\gamma}_Km_{12}\right|+\mu_1\overline{\beta}_K^2\overline{\gamma}_K^2,\end{aligned}$$

leads to

$$\zeta_1\zeta_2-\zeta_3^2\geq\zeta_1^{HW}\zeta_2^{HW}-m_{12}^2.$$

Thus, (**H1**) implies (**A1**), but not vice versa. For example, if $\overline{\beta}_K=0$ and $\overline{\gamma}_K\neq 0$ (i.e., trapezoidal mesh), then we find that (**A1**) cannot imply (**H1**). The proof is complete. □

Here, we give a specific example, such that the assumption (**A1**) is satisfied, but (**H1**) fails. Let the four vertices of K given by $(0,0)^T$, $(10,0)^T$, $(1,1)^T$, and $(0,1)^T$, and assume that Λ_K is the identity matrix. Then, by some direct calculations, we have $\zeta_1\zeta_2-\zeta_3^2=0.0119$, while $\zeta_1^{HW}\zeta_2^{HW}-m_{12}^2=-0.0957$. To close this section, we employ some special meshes to explore the meaning of (**A1**), including the parallelogram and $h^{1+\gamma}$-parallelogram meshes.

Theorem 3.3. *Suppose that $\mathcal{T}_h$ consists of parallelograms, then* (**A1**) *holds with*

$$\varrho=\min_{K\in\mathcal{T}_h}\left[\frac{1}{16}\det(\Lambda_K)\right]\geq\frac{1}{16}\underline{\lambda}^2.$$

Proof. If $K\in\mathcal{T}_h$ is a parallelogram, then we obtain $\boldsymbol{m}_K=\mathbf{0}$ and $\overline{\beta}_K=\overline{\gamma}_K=0$. It follows from Eqs (3.3) and (3.6) that

$$\zeta_1\zeta_2-\zeta_3^2=m_{11}m_{22}-m_{12}^2=\frac{1}{16}\det(\Lambda_K),\quad\forall\,K\in\mathcal{T}_h,$$

implying the desired result. □

Theorem 3.4. *Assume that $\mathcal{T}_h$ consists of $h^{1+\gamma}$-parallelograms, i.e., $\|\boldsymbol{m}_K\|\lesssim h_K^{1+\gamma}$, $\forall\,K\in\mathcal{T}_h$, where $\gamma>0$ is a constant. Let Eq* (2.4) *hold. Then, when h is small enough, we have*

$$\left|\left(\zeta_1\zeta_2-\zeta_3^2\right)-\frac{1}{16}\det\left(\Lambda_K\right)\right|\lesssim h_K^{2\gamma},\quad\forall\,K\in\mathcal{T}_h.$$

As a result, (**A1**) *holds with $\varrho=C_0\underline{\lambda}^2$, where $0<C_0<1/16$ is a constant.*

Proof. By denoting

$$a_1=-\frac{\mu_3^2}{16\mu_1}\overline{\beta}_K^2,\quad a_2=-\frac{\mu_2^2}{16\mu_1}\overline{\gamma}_K^2,\quad a_3=\frac{\mu_2\mu_3}{16\mu_1}\overline{\beta}_K\overline{\gamma}_K,$$

we obtain

$$\zeta_1\zeta_2-\zeta_3^2=\frac{1}{16}\det(\Lambda_K)+Res,\quad Res=a_2m_{11}+a_1m_{22}+a_1a_2-2a_3m_{12}-a_3^2.$$

Since $\mathcal{T}_h$ is an $h^{1+\gamma}$-parallelogram mesh and Eq (2.4) holds, we deduce that $\left|\overline{\beta}_K\right|\lesssim h_K^{\gamma}$, $\left|\overline{\gamma}_K\right|\lesssim h_K^{\gamma}$, and $\mu_i\lesssim 1\,(i=2,3)$. It follows that $|a_i|\lesssim h_K^{2\gamma}\,(i=1,2,3)$ and $|Res|\lesssim h_K^{2\gamma}$, completing the proof. □

4. Error analysis

In this section, for any adjacent elements K_1 and K_2 with a common edge, we assume that $\|\Lambda_{K_1} - \Lambda_{K_2}\| \lesssim h$. The quadrilateral mesh $\mathcal{T}_h$ is called h^2-uniform (c.f. [12, 27]) provided that the relation $\|\boldsymbol{m}_K\| \lesssim h_K^2$, $\forall\, K \in \mathcal{T}_h$ holds, and for any two adjacent quadrilateral elements $K_1 = \square \boldsymbol{x}_1\boldsymbol{x}_2\boldsymbol{x}_3\boldsymbol{x}_4$ and $K_2 = \square \boldsymbol{x}_4\boldsymbol{x}_3\boldsymbol{x}_5\boldsymbol{x}_6$ (see Figure 3), they satisfy the h^2-parallelogram condition $\|2\boldsymbol{x}_4 - \boldsymbol{x}_1 - \boldsymbol{x}_6\| \lesssim h^2$.

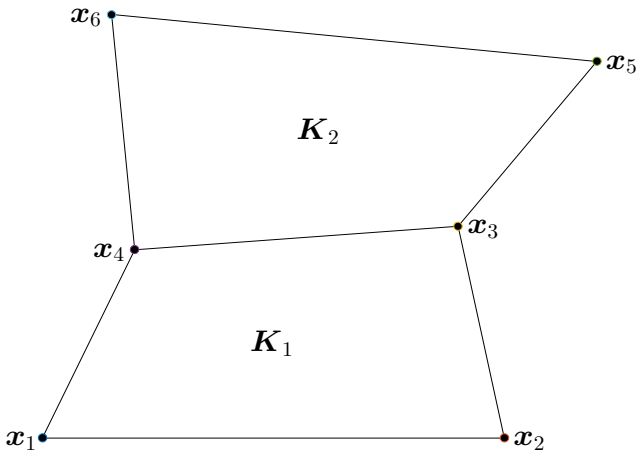

Figure 3. Two adjacent quadrilaterals $K_1 = \square \boldsymbol{x}_1\boldsymbol{x}_2\boldsymbol{x}_3\boldsymbol{x}_4$ and $K_2 = \square \boldsymbol{x}_4\boldsymbol{x}_3\boldsymbol{x}_5\boldsymbol{x}_6$ that have the common edge $\boldsymbol{x}_4\boldsymbol{x}_3$.

4.1. Superconvergence

Denote by $u_I \in U_h$ the isoparametric bilinear interpolation of u, such that $u_I(\boldsymbol{x}_i) = u(\boldsymbol{x}_i)$, $\forall\, \boldsymbol{x}_i \in \mathcal{N}_h$. Then, we have the following superconvergence result (4.1).

Lemma 4.1. *[20, 39, 50] Let the quadrilateral mesh $\mathcal{T}_h$ be h^2-uniform, then we have*

$$\left\|\overline{\nabla}(u - u_I)(\boldsymbol{x})\right\| \lesssim h^2\|u\|_{3,\infty}, \quad \forall\, u \in W^{3,\infty}(\Omega), \tag{4.1}$$

where $\overline{\nabla}$ is the arithmetic average of the gradient over all neighboring quadrilateral elements for $\boldsymbol{x}$, while $\boldsymbol{x}$ is any geometric center in C_h, or any interior vertex in $\mathcal{N}_h^\circ$, or any interior midpoint in $\mathcal{M}_h^\circ$.

It follows from Eq (3.4) that

$$|u_I - u_h|_1^2 \lesssim \widetilde{a}_h\left(u_I - u_h, (u_I - u_h)^*\right) = J_1 + J_2, \tag{4.2}$$

where

$$J_1 = \widetilde{a}_h\left(u_I - u, (u_I - u_h)^*\right), \quad J_2 = \widetilde{a}_h\left(u - u_h, (u_I - u_h)^*\right).$$

Next, we will analyze the right-hand side of Eq (4.2) term by term.

Lemma 4.2. *Let $u \in H_0^1(\Omega) \cap W^{3,\infty}(\Omega)$ be the exact solution of Eqs* (2.1) *and* (2.2)*, and $u_h \in U_h$ be the finite volume element solution of Eq* (2.7)*. Assume that the quadrilateral mesh $\mathcal{T}_h$ is h^2-uniform, then we have*

$$|J_1| \lesssim h^2\|u\|_{3,\infty}|u_I - u_h|_1. \tag{4.3}$$

Proof. Let

$$\widetilde{a}_{1,K,h}(u_h, v_h) = \frac{1}{2}\sum_{i=1}^{4}[v_h]_{\boldsymbol{x}_K\boldsymbol{y}_i}(\boldsymbol{x}_K - \boldsymbol{y}_i)^T\mathcal{R}^T\Lambda_K\nabla u_h(\boldsymbol{x}_K),$$

$$\widetilde{a}_{2,K,h}(u_h, v_h) = \frac{1}{2}\sum_{i=1}^{4}[v_h]_{\boldsymbol{x}_K\boldsymbol{y}_i}(\boldsymbol{x}_K - \boldsymbol{y}_i)^T\mathcal{R}^T\Lambda_K\nabla u_h(\boldsymbol{y}_i),$$

then we have $\widetilde{a}_{K,h}(u_h, v_h) = \widetilde{a}_{1,K,h}(u_h, v_h) + \widetilde{a}_{2,K,h}(u_h, v_h)$. In the following, we will estimate the terms $\widetilde{a}_{1,K,h}(\cdot,\cdot)$ and $\widetilde{a}_{2,K,h}(\cdot,\cdot)$ one by one. First, by Eq (4.1) and Cauchy-Schwarz inequality,

$$\begin{aligned}\sum_{K\in\mathcal{T}_h}\left|\widetilde{a}_{1,K,h}(u-u_I,(u_I-u_h)^*)\right| &= \frac{1}{2}\sum_{K\in\mathcal{T}_h}\left|\sum_{i=1}^{4}[(u_I-u_h)^*]_{\boldsymbol{x}_K\boldsymbol{y}_i}(\boldsymbol{x}_K-\boldsymbol{y}_i)^T\mathcal{R}^T\Lambda_K\nabla(u-u_I)(\boldsymbol{x}_K)\right| \\ &\lesssim \sum_{K\in\mathcal{T}_h}\sum_{i=1}^{4}h|u_I-u_h|_{1,K,h}\,\|\nabla(u-u_I)(\boldsymbol{x}_K)\| \\ &\lesssim h^3\|u\|_{3,\infty}\sum_{K\in\mathcal{T}_h}|u_I-u_h|_{1,K,h} \\ &\lesssim h^2\|u\|_{3,\infty}|u_I-u_h|_1,\end{aligned}$$

where $|u_h|_{1,K,h} = \|\delta\boldsymbol{U}_K\|$; also, we have used the fact that the number of elements in $\mathcal{T}_h$ is $\mathcal{O}(h^{-2})$. Second, for any two adjacent quadrilateral elements $K_1, K_2 \in \mathcal{T}_h$, we assume that the common edge of K_1 and K_2 is $\boldsymbol{x}_i\boldsymbol{x}_j \in \mathcal{E}_h^\circ$; see Figure 4. Moreover, we let $\boldsymbol{y}_{ij}$ be the midpoint of $\boldsymbol{x}_i\boldsymbol{x}_j$. It can be checked that $\|2\boldsymbol{y}_{ij} - \boldsymbol{x}_{K_1} - \boldsymbol{x}_{K_2}\| \lesssim h^2$. By noticing $(u_I - u_h)^* = 0$ on $\partial\Omega$, it follows from Eq (4.1) that

$$\begin{aligned}\left|\sum_{K\in\mathcal{T}_h}\widetilde{a}_{2,K,h}(u-u_I,(u_I-u_h)^*)\right| &= \Bigg|\sum_{\boldsymbol{x}_i\boldsymbol{x}_j\in\mathcal{E}_h^\circ}[(u_I-u_h)^*]_{\boldsymbol{x}_{K_1}\boldsymbol{x}_{K_2}}\frac{1}{2}\Big((\boldsymbol{x}_{K_1}-\boldsymbol{y}_{ij})^T\mathcal{R}^T\Lambda_{K_1}\nabla_{K_1}(u-u_I)(\boldsymbol{y}_{ij}) \\ &\quad + (\boldsymbol{y}_{ij}-\boldsymbol{x}_{K_2})^T\mathcal{R}^T\Lambda_{K_2}\nabla_{K_2}(u-u_I)(\boldsymbol{y}_{ij})\Big)\Bigg| \\ &= \Bigg|\sum_{\boldsymbol{x}_i\boldsymbol{x}_j\in\mathcal{E}_h^\circ}[(u_I-u_h)^*]_{\boldsymbol{x}_{K_1}\boldsymbol{x}_{K_2}}\frac{1}{2}\Big((\boldsymbol{x}_{K_1}-\boldsymbol{y}_{ij})^T\mathcal{R}^T\Lambda_{K_1}\nabla_{K_1}(u-u_I)(\boldsymbol{y}_{ij}) \\ &\quad + (\boldsymbol{x}_{K_1}-\boldsymbol{y}_{ij})^T\mathcal{R}^T\Lambda_{K_2}\nabla_{K_2}(u-u_I)(\boldsymbol{y}_{ij}) \\ &\quad + (2\boldsymbol{y}_{ij}-\boldsymbol{x}_{K_1}-\boldsymbol{x}_{K_2})^T\mathcal{R}^T\Lambda_{K_2}\nabla_{K_2}(u-u_I)(\boldsymbol{y}_{ij})\Big)\Bigg| \\ &\lesssim \sum_{\boldsymbol{x}_i\boldsymbol{x}_j\in\mathcal{E}_h^\circ}|u_I-u_h|_{1,K_1,h}\left(h\left\|\overline{\nabla}(u-u_I)(\boldsymbol{y}_{ij})\right\| + h^2\left\|\nabla_{K_2}(u-u_I)(\boldsymbol{y}_{ij})\right\|\right) \\ &\lesssim h^3\|u\|_{3,\infty}\sum_{\boldsymbol{x}_i\boldsymbol{x}_j\in\mathcal{E}_h^\circ}|u_I-u_h|_{1,K_1,h} \\ &\lesssim h^2\|u\|_{3,\infty}|u_I-u_h|_1,\end{aligned}$$

where ∇_{K_i} is the gradient ∇ that restricts on K_i, $i = 1, 2$,

$$[(u_I-u_h)^*]_{\boldsymbol{x}_{K_1}\boldsymbol{x}_{K_2}} = (u_I-u_h)(\boldsymbol{x}_j) - (u_I-u_h)(\boldsymbol{x}_i),$$

$$\left\|\Lambda_{K_1}\nabla_{K_1}(u-u_I)(\boldsymbol{y}_{ij})+\Lambda_{K_2}\nabla_{K_2}(u-u_I)(\boldsymbol{y}_{ij})\right\| = \left\|2\Lambda_{K_1}\overline{\nabla}(u-u_I)(\boldsymbol{y}_{ij})+(\Lambda_{K_2}-\Lambda_{K_1})\nabla_{K_2}(u-u_I)(\boldsymbol{y}_{ij})\right\|$$
$$\lesssim \left\|\overline{\nabla}(u-u_I)(\boldsymbol{y}_{ij})\right\| + h\left\|\nabla_{K_2}(u-u_I)(\boldsymbol{y}_{ij})\right\|,$$

and we have used the fact that $\left\|\nabla_{K_2}(u-u_I)(\boldsymbol{y}_{ij})\right\| \lesssim h\|u\|_{3,\infty}$, which can be obtained by Taylor's expansion; the proof is similar to [39] and we omit it here. Consequently,

$$|\widetilde{a}_h(u-u_I,(u_I-u_h)^*)| \le \sum_{K\in\mathcal{T}_h}\left|\widetilde{a}_{1,K,h}(u-u_I,(u_I-u_h)^*)\right| + \left|\sum_{K\in\mathcal{T}_h}\widetilde{a}_{2,K,h}(u-u_I,(u_I-u_h)^*)\right|$$
$$\lesssim h^2\|u\|_{3,\infty}|u_I-u_h|_1,$$

leads to Eq (4.3) and completes the proof. □

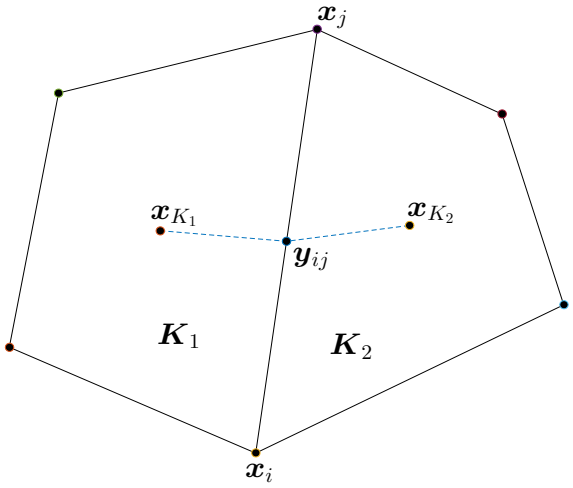

Figure 4. Two adjacent quadrilateral elements K_1 and K_2 that have a common edge $\boldsymbol{x}_i\boldsymbol{x}_j$.

Lemma 4.3. *Assume that $u \in H_0^1(\Omega)\cap W^{3,\infty}(\Omega)$ is the exact solution of Eqs* (2.1) *and* (2.2)*, and $u_h \in U_h$ is the finite volume element solution of Eq* (2.7)*. Then, we have*

$$|J_2| \lesssim h^2\|u\|_{3,\infty}|u_I-u_h|_1. \tag{4.4}$$

Proof. By Eqs (2.5) and (2.7), we deduce that $a_h(u,v_h) = (f,v_h) = \widetilde{a}_h(u_h,v_h)$, $\forall\, v_h \in V_h$. From Eqs (2.6) and (2.8), and using the quadrature error of trapezoidal rule, we have

$$|\widetilde{a}_h(u-u_h,(u_I-u_h)^*)| = |\widetilde{a}_h(u,(u_I-u_h)^*) - a_h(u,(u_I-u_h)^*)|$$
$$= \left|\sum_{K\in\mathcal{T}_h}\sum_{i=1}^{4}[(u_I-u_h)^*]_{\boldsymbol{x}_K\boldsymbol{y}_i}E_{K,i}\right|$$
$$\lesssim \sum_{K\in\mathcal{T}_h}\sum_{i=1}^{4}h_K^3|u_I-u_h|_{1,K,h}\|u\|_{3,\infty,K}$$
$$\lesssim h^3\|u\|_{3,\infty}\sum_{K\in\mathcal{T}_h}|u_I-u_h|_{1,K,h}$$
$$\lesssim h^2\|u\|_{3,\infty}|u_I-u_h|_1,$$

where

$$E_{K,i} = \int_{\boldsymbol{x}_K \boldsymbol{y}_i} (-\Lambda_K \nabla u) \cdot \boldsymbol{n}^*_{K,i} \, \mathrm{d}s - \frac{1}{2}(\boldsymbol{x}_K - \boldsymbol{y}_i)^T \mathcal{R}^T \Lambda_K \left[\nabla u(\boldsymbol{x}_K) + \nabla u(\boldsymbol{y}_i)\right].$$

The proof is complete. □

Theorem 4.1. *Suppose that the quadrilateral mesh $\mathcal{T}_h$ is regular and h^2-uniform. Let $u \in H_0^1(\Omega) \cap W^{3,\infty}(\Omega)$ be the exact solution of Eqs* (2.1) *and* (2.2)*, and $u_h \in U_h$ is the finite volume element solution of Eq* (2.7)*. Then, we have*

$$|u_I - u_h|_1 \lesssim h^2 \|u\|_{3,\infty}. \tag{4.5}$$

Proof. Combining the results Eqs (4.2)–(4.4), we obtain Eq (4.5). □

4.2. Some corollaries

Corollary 4.1. *Under the same assumptions as in Theorem 4.1, we have*

$$|u - u_h|_1 \lesssim h\|u\|_{3,\infty}$$

and

$$\|u - u_h\|_0 \lesssim h^2 \|u\|_{3,\infty}. \tag{4.6}$$

Proof. Recalling the triangle inequality, standard interpolation error estimate, and Eq (4.5),

$$|u - u_h|_1 \le |u - u_I|_1 + |u_I - u_h|_1 \lesssim h\|u\|_{3,\infty},$$

and by Poincaré-Friedrichs inequality,

$$\|u - u_h\|_0 \le \|u - u_I\|_0 + \|u_I - u_h\|_0 \lesssim \|u - u_I\|_0 + |u_I - u_h|_1 \lesssim h^2\|u\|_{3,\infty},$$

which completes the proof. □

In the above optimal L^2 error estimate, we do not use the Aubin-Nitsche technique, and Eq (4.6) is a by-product of the superconvergence result (4.5).

Corollary 4.2. *Under the same assumptions as in Theorem 4.1, we have*

$$\left(\frac{1}{\#S}\sum_{\boldsymbol{x}\in S}\left\|\overline{\nabla}(u - u_h)(\boldsymbol{x})\right\|^2\right)^{\frac{1}{2}} \lesssim h^2\|u\|_{3,\infty}, \tag{4.7}$$

where S is the set C_h or $\mathcal{N}_h^\circ$ or $\mathcal{M}_h^\circ$, and $\#S$ denotes the cardinality of S.

Proof. It follows from Eq (4.1) that

$$\left(\frac{1}{\#S}\sum_{\boldsymbol{x}\in S}\left\|\overline{\nabla}(u - u_I)(\boldsymbol{x})\right\|^2\right)^{\frac{1}{2}} \lesssim h^2\|u\|_{3,\infty}\left(\frac{1}{\#S}\sum_{\boldsymbol{x}\in S} 1\right)^{\frac{1}{2}} \lesssim h^2\|u\|_{3,\infty}.$$

By using the inverse inequality, the fact $\#S = O(h^{-2})$, and Eq (4.5),

$$\begin{aligned}\left(\frac{1}{\#S}\sum_{\boldsymbol{x}\in S}\left\|\overline{\nabla}(u_I - u_h)(\boldsymbol{x})\right\|^2\right)^{\frac{1}{2}} &\lesssim \left(\frac{1}{\#S}\sum_{\boldsymbol{x}\in S} h^{-2}\|u_I - u_h\|^2_{1,K_{\boldsymbol{x}}}\right)^{\frac{1}{2}} \lesssim \left(\sum_{\boldsymbol{x}\in S}\|u_I - u_h\|^2_{1,K_{\boldsymbol{x}}}\right)^{\frac{1}{2}} \\ &\lesssim \|u_I - u_h\|_1 \lesssim h^2\|u\|_{3,\infty},\end{aligned}$$

where $K_{\boldsymbol{x}} = \cup_{K'\ni \boldsymbol{x}}\{K'\}$ is the union of quadrilateral element K' that contains $\boldsymbol{x}$. Thus, we get the desired result (4.7) by combining the above results. □

5. Numerical results

Several numerical examples are given in this section to verify the above theoretical results, in which we use four types of meshes. The first type (Mesh I) is a uniform rectangular mesh, see Figure 5(a), where the coordinates of the vertices are given by

$$h(i-1, j-1)^T, \quad 1 \le i,\ j \le n+1,$$

and $h = 1/n$ is the mesh size. The second one (Mesh II) is a quadrilateral mesh constructed by disturbing the vertices of Mesh I and keeping the connections unchanged, see Figure 5(b), where the coordinates of the vertices are subjected to

$$x_{ij} = (i-1)h,\ y_{ij} = (j-1)h + \frac{1}{25}\sin(2\pi h(i-1))\sin(2\pi h(j-1)), \quad 1 \le i,\ j \le n+1.$$

Mesh IV is a uniform trapezoidal mesh also obtained by disturbing some vertices of Mesh I, see Figure 5(d), where the disturbance of a vertex is $h/4$ along y direction. For Meshes I, II, and IV, we set $\Omega = (0,1)^2$ in the following numerical examples. The third mesh (Mesh III), see Figure 5(c), is a refined one where the initial region Ω_0 is a quadrilateral, and the four coordinates of Ω_0 are given as below

$$(0,0)^T, \quad (1,0)^T, \quad (0.8,1)^T, \quad (0.2,1)^T.$$

Precisely, Mesh III is obtained by the standard bisection procedure, i.e., by connecting the midpoints of opposite edges of each quadrilateral; see the thin line segments of Figure 5(c). It can be verified that Meshes I, II, and III are all h^2-uniform. For convenience, we denote

$$E_C = \left(\frac{1}{\#C_h}\sum_{\boldsymbol{x}\in C_h}\left\|\overline{\nabla}(u-u_h)(\boldsymbol{x})\right\|^2\right)^{\frac{1}{2}}, \quad E_{\mathcal{V}} = \left(\frac{1}{\#\mathcal{N}_h^\circ}\sum_{\boldsymbol{x}\in \mathcal{N}_h^\circ}\left\|\overline{\nabla}(u-u_h)(\boldsymbol{x})\right\|^2\right)^{\frac{1}{2}}$$

and

$$E_{\mathcal{M}} = \left(\frac{1}{\#\mathcal{M}_h^\circ}\sum_{\boldsymbol{x}\in \mathcal{M}_h^\circ}\left\|\overline{\nabla}(u-u_h)(\boldsymbol{x})\right\|^2\right)^{\frac{1}{2}}$$

as the errors at geometric centers, interior vertices, and edge midpoints, respectively. Moreover, for the ζ_i that appears in Eq (3.3), we define

$$\varrho = \min_{K\in\mathcal{T}_h}\left\{\zeta_1\zeta_2 - \zeta_3^2\right\}.$$

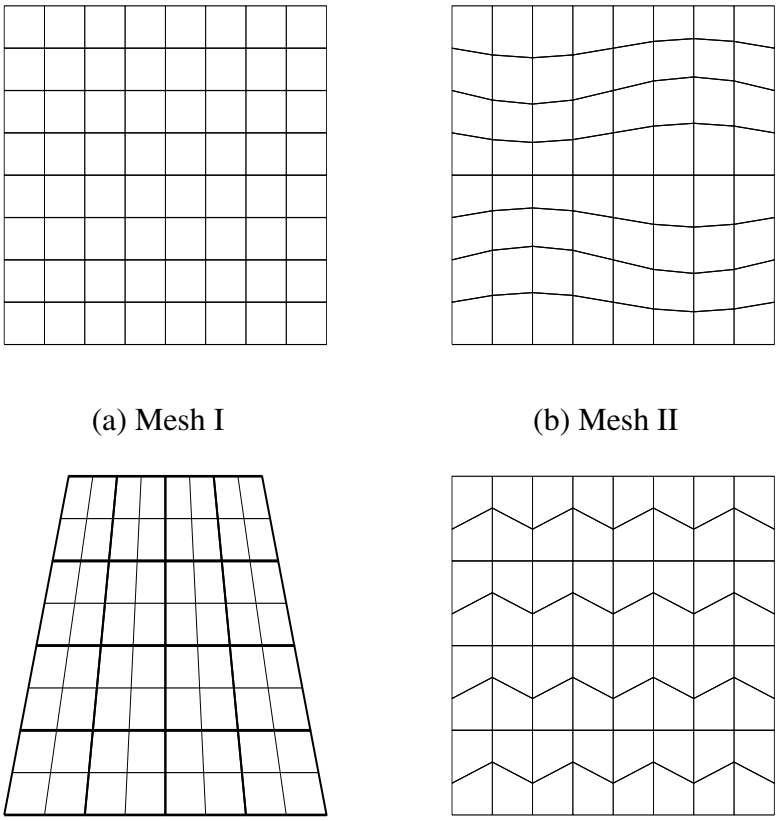

(a) Mesh I (b) Mesh II

(c) Mesh III (d) Mesh IV

Figure 5. Mesh types used in the numerical experiments.

Example 5.1. *Solve Eqs* (2.1) *and* (2.2)*, and choose the anisotropic diffusion coefficient and right-hand side function as follows:*

$$\Lambda = \begin{pmatrix} 1 & 1 \\ 1 & 2 \end{pmatrix}, \quad f(x, y) = -5e^{x+y}.$$

This problem has the analytic solution $u(x, y) = e^{x+y}$.

The numerical results are reported in Tables 1 and 2, where "Order" indicates the numerical convergence order computed by $\log_2(E_{2h}/E_h)$, where E_{2h} and E_h are the errors of the corresponding two successive mesh sizes $\mathcal{T}_{2h}$ and $\mathcal{T}_h$. One can see that, for the four meshes and diffusion coefficient, (**A1**) is satisfied. In particular, for Meshes I, II, and III, the finite volume element solution u_h converges to the interpolation u_I of u with second-order under H^1 norm, which conforms the superconvergence property in Theorem 4.1. The remaining results of these two tables also verify the theoretical findings in Corollaries 4.1 and 4.2. Note that Mesh IV is not h^2-uniform; then, the corresponding finite volume element solution does not preserve the superconvergence result.

Table 1. Numerical results for Example 5.1 on Meshes I and II.

Mesh	$\#\mathcal{T}_h$	8×8	16×16	32×32	64×64	128×128	256×256
Mesh I	ϱ	6.25e-02	6.25e-02	6.25e-02	6.25e-02	6.25e-02	6.25e-02
	$\lvert u_I - u_h\rvert_1$	5.35e-03	1.38e-03	3.48e-04	8.73e-05	2.18e-05	5.46e-06
	Order	/	1.96	1.99	2.00	2.00	2.00
	$\lvert u - u_h\rvert_1$	1.63e-01	8.15e-02	4.08e-02	2.04e-02	1.02e-02	5.09e-03
	Order	/	1.00	1.00	1.00	1.00	1.00
	$\lVert u - u_h\rVert_0$	9.60e-03	2.41e-03	6.03e-04	1.51e-04	3.77e-05	9.42e-06
	Order	/	1.99	2.00	2.00	2.00	2.00
	E_C	1.17e-02	2.94e-03	7.36e-04	1.84e-04	4.60e-05	1.15e-05
	Order	/	1.99	2.00	2.00	2.00	2.00
	$E_{\mathcal{V}}$	2.80e-02	7.07e-03	1.78e-03	4.46e-04	1.12e-04	2.79e-05
	Order	/	1.98	1.99	2.00	2.00	2.00
	$E_{\mathcal{M}}$	1.98e-02	4.98e-03	1.25e-03	3.13e-04	7.82e-05	1.95e-05
	Order	/	1.99	2.00	2.00	2.00	2.00
Mesh II	ϱ	6.25e-02	6.25e-02	6.25e-02	6.25e-02	6.25e-02	6.25e-02
	$\lvert u_I - u_h\rvert_1$	1.07e-02	3.11e-03	8.15e-04	2.06e-04	5.18e-05	1.30e-05
	Order	/	1.78	1.93	1.98	1.99	2.00
	$\lvert u - u_h\rvert_1$	1.67e-01	8.38e-02	4.19e-02	2.10e-02	1.05e-02	5.24e-03
	Order	/	1.00	1.00	1.00	1.00	1.00
	$\lVert u - u_h\rVert_0$	9.43e-03	2.37e-03	5.95e-04	1.49e-04	3.72e-05	9.30e-06
	Order	/	1.99	2.00	2.00	2.00	2.00
	E_C	1.68e-02	4.44e-03	1.13e-03	2.84e-04	7.12e-05	1.78e-05
	Order	/	1.92	1.97	1.99	2.00	2.00
	$E_{\mathcal{V}}$	7.85e-02	2.29e-02	5.99e-03	1.52e-03	3.83e-04	9.60e-05
	Order	/	1.78	1.93	1.98	1.99	2.00
	$E_{\mathcal{M}}$	6.90e-02	1.78e-02	4.46e-03	1.11e-03	2.78e-04	6.94e-05
	Order	/	1.95	2.00	2.00	2.00	2.00

Table 2. Numerical results for Example 5.1 on Meshes III and IV.

Mesh	$\#\mathcal{T}_h$	8×8	16×16	32×32	64×64	128×128	256×256
Mesh III	ϱ	6.25e-02	6.25e-02	6.25e-02	6.25e-02	6.25e-02	6.25e-02
	$\lvert u_I - u_h\rvert_1$	5.51e-04	1.46e-04	3.70e-05	9.31e-06	2.33e-06	5.83e-07
	Order	/	1.92	1.97	1.99	2.00	2.00
	$\lvert u - u_h\rvert_1$	1.16e-01	5.82e-02	2.91e-02	1.46e-02	7.28e-03	3.64e-03
	Order	/	1.00	1.00	1.00	1.00	1.00
	$\lVert u - u_h\rVert_0$	5.49e-03	1.37e-03	3.43e-04	8.58e-05	2.14e-05	5.36e-06
	Order	/	2.00	2.00	2.00	2.00	2.00
	E_C	2.20e-03	5.54e-04	1.39e-04	3.47e-05	8.68e-06	2.17e-06
	Order	/	1.99	2.00	2.00	2.00	2.00
	$E_{\mathcal{V}}$	8.30e-03	2.09e-03	5.25e-04	1.32e-04	3.29e-05	8.23e-06
	Order	/	1.99	1.99	2.00	2.00	2.00
	$E_{\mathcal{M}}$	6.21e-03	1.58e-03	3.97e-04	9.96e-05	2.50e-05	6.25e-06
	Order	/	1.98	1.99	1.99	2.00	2.00
Mesh IV	ϱ	6.23e-02	6.23e-02	6.23e-02	6.23e-02	6.23e-02	6.23e-02
	$\lvert u_I - u_h\rvert_1$	1.04e-02	3.74e-03	1.59e-03	7.56e-04	3.74e-04	1.86e-04
	Order	/	1.48	1.23	1.07	1.02	1.00
	$\lvert u - u_h\rvert_1$	1.86e-01	9.42e-02	4.74e-02	2.38e-02	1.19e-02	5.95e-03
	Order	/	0.98	0.99	1.00	1.00	1.00
	$\lVert u - u_h\rVert_0$	1.07e-02	2.72e-03	6.86e-04	1.72e-04	4.32e-05	1.08e-05
	Order	/	1.97	1.99	1.99	2.00	2.00
	E_C	7.14e-02	3.55e-02	1.77e-02	8.87e-03	4.43e-03	2.22e-03
	Order	/	1.01	1.00	1.00	1.00	1.00
	$E_{\mathcal{V}}$	1.55e-01	7.62e-02	3.78e-02	1.88e-02	9.38e-03	4.69e-03
	Order	/	1.02	1.01	1.01	1.00	1.00
	$E_{\mathcal{M}}$	6.99e-02	3.51e-02	1.76e-02	8.82e-03	4.42e-03	2.21e-03
	Order	/	0.99	1.00	1.00	1.00	1.00

Example 5.2. *We still consider the problem Eqs* (2.1) *and* (2.2) *with the following discontinuous anisotropic diffusion coefficient:*

$$\Lambda(x,y) = \begin{cases} \begin{pmatrix} 1.75 & 0.5 \\ 0.5 & 1.75 \end{pmatrix}, & x \le 0.5, \\ \begin{pmatrix} 3 & 1 \\ 1 & 2 \end{pmatrix}, & x > 0.5. \end{cases}$$

The exact solution and corresponding right-hand side function are given by

$$u(x,y)=\begin{cases}2xe^{y}, & x\le 0.5,\\ (0.5+x)e^{y}, & x>0.5,\end{cases}\qquad f(x,y)=\begin{cases}-(2+3.5x)e^{y}, & x\le 0.5,\\ -(3+2x)e^{y}, & x>0.5.\end{cases}$$

We mention that, in this example, $u \notin W^{3,\infty}(\Omega)$, and u is just a continuous function. Moreover, the first derivative $(\Lambda\nabla u)\cdot \boldsymbol{n}$ on the interface $x = 0.5$ is a continuous vector-valued function. We can observe from Tables 3 and 4 that the numerical results are similar to the previous example, except the convergence orders of $E_{\mathcal{V}}$ and $E_{\mathcal{M}}$, which are all approximately 1.5 (the corresponding superconvergence results have not been proved for the discontinuous anisotropic diffusion coefficient), and a little lower than 2.

Example 5.3. *Solve a highly anisotropic diffusion problem that was considered in [3], where the diffusion coefficient and analytic solution are as follows:*

$$\Lambda=\begin{pmatrix}\cos\theta & \sin\theta\\ -\sin\theta & \cos\theta\end{pmatrix}\begin{pmatrix}1 & 0\\ 0 & \kappa\end{pmatrix}\begin{pmatrix}\cos\theta & -\sin\theta\\ \sin\theta & \cos\theta\end{pmatrix},\quad u(x,y)=\frac{\arctan\left(0.5-(x-0.5)^2-(y-0.5)^2\right)}{\arctan 0.5},$$

respectively. Thus, the right-hand side function is given by

$$\begin{aligned}f(x,y)=&\frac{2}{\left(1+f_1^2(x,y)\right)^2\arctan 0.5}\Big((\kappa+1)\left(1+f_1^2(x,y)\right)+8(\kappa-1)(x-0.5)(y-0.5)f_1(x,y)\sin\theta\cos\theta\\ &+4f_1(x,y)\left((x-0.5)^2\left(\kappa\sin^2\theta+\cos^2\theta\right)+(y-0.5)^2\left(\sin^2\theta+\kappa\cos^2\theta\right)\right)\Big),\end{aligned}$$

with $f_1(x,y)=x+y-x^2-y^2$. In this example, we employ $\kappa=10^3$ and $\theta=\pi/4$.

Table 3. Numerical results for Example 5.2 on Meshes I and II.

Mesh	$\#\mathcal{T}_h$	8×8	16×16	32×32	64×64	128×128	256×256
Mesh I	ϱ	1.76e-01	1.76e-01	1.76e-01	1.76e-01	1.76e-01	1.76e-01
	$\lvert u_I - u_h\rvert_1$	8.43e-04	2.14e-04	5.38e-05	1.35e-05	3.37e-06	8.42e-07
	Order	/	1.98	1.99	2.00	2.00	2.00
	$\lvert u - u_h\rvert_1$	6.32e-02	3.16e-02	1.58e-02	7.89e-03	3.95e-03	1.97e-03
	Order	/	1.00	1.00	1.00	1.00	1.00
	$\lVert u - u_h\rVert_0$	2.62e-03	6.57e-04	1.64e-04	4.11e-05	1.03e-05	2.57e-06
	Order	/	2.00	2.00	2.00	2.00	2.00
	E_C	5.80e-03	1.45e-03	3.63e-04	9.09e-05	2.27e-05	5.68e-06
	Order	/	2.00	2.00	2.00	2.00	2.00
	$E_{\mathcal{V}}$	2.23e-02	7.47e-03	2.56e-03	8.89e-04	3.11e-04	1.10e-04
	Order	/	1.58	1.55	1.53	1.51	1.51
	$E_{\mathcal{M}}$	1.74e-02	5.57e-03	1.86e-03	6.38e-04	2.22e-04	7.78e-05
	Order	/	1.64	1.58	1.54	1.52	1.51
Mesh II	ϱ	1.76e-01	1.76e-01	1.76e-01	1.76e-01	1.76e-01	1.76e-01
	$\lvert u_I - u_h\rvert_1$	4.86e-03	1.34e-03	3.43e-04	8.61e-05	2.16e-05	5.39e-06
	Order	/	1.86	1.97	1.99	2.00	2.00
	$\lvert u - u_h\rvert_1$	6.88e-02	3.46e-02	1.73e-02	8.66e-03	4.33e-03	2.16e-03
	Order	/	0.99	1.00	1.00	1.00	1.00
	$\lVert u - u_h\rVert_0$	2.74e-03	6.89e-04	1.72e-04	4.31e-05	1.08e-05	2.70e-06
	Order	/	1.99	2.00	2.00	2.00	2.00
	E_C	1.01e-02	2.58e-03	6.49e-04	1.63e-04	4.06e-05	1.02e-05
	Order	/	1.97	1.99	2.00	2.00	2.00
	$E_{\mathcal{V}}$	5.03e-02	1.53e-02	4.35e-03	1.26e-03	3.87e-04	1.24e-04
	Order	/	1.72	1.82	1.78	1.71	1.64
	$E_{\mathcal{M}}$	4.17e-02	1.14e-02	3.12e-03	8.97e-04	2.73e-04	8.80e-05
	Order	/	1.87	1.87	1.80	1.71	1.64

Table 4. Numerical results for Example 5.2 on Meshes III and IV.

Mesh	$\#\mathcal{T}_h$	8×8	16×16	32×32	64×64	128×128	256×256
Mesh III	ϱ	1.76e-01	1.76e-01	1.76e-01	1.76e-01	1.76e-01	1.76e-01
	$\lvert u_I - u_h\rvert_1$	3.07e-04	7.79e-05	1.96e-05	4.90e-06	1.22e-06	3.06e-07
	Order	/	1.98	1.99	2.00	2.00	2.00
	$\lvert u - u_h\rvert_1$	5.58e-02	2.79e-02	1.39e-02	6.97e-03	3.49e-03	1.74e-03
	Order	/	1.00	1.00	1.00	1.00	1.00
	$\lVert u - u_h\rVert_0$	2.24e-03	5.61e-04	1.40e-04	3.51e-05	8.77e-06	2.19e-06
	Order	/	2.00	2.00	2.00	2.00	2.00
	E_C	1.58e-03	3.97e-04	9.94e-05	2.49e-05	6.22e-06	1.55e-06
	Order	/	1.99	2.00	2.00	2.00	2.00
	$E_{\mathcal{V}}$	7.57e-03	2.61e-03	9.01e-04	3.14e-04	1.10e-04	3.87e-05
	Order	/	1.54	1.53	1.52	1.51	1.51
	$E_{\mathcal{M}}$	6.26e-03	2.00e-03	6.65e-04	2.27e-04	7.87e-05	2.75e-05
	Order	/	1.64	1.59	1.55	1.53	1.51
Mesh IV	ϱ	1.75e-01	1.75e-01	1.75e-01	1.75e-01	1.75e-01	1.75e-01
	$\lvert u_I - u_h\rvert_1$	8.76e-03	4.32e-03	2.16e-03	1.08e-03	5.43e-04	2.72e-04
	Order	/	1.02	1.00	1.00	1.00	1.00
	$\lvert u - u_h\rvert_1$	9.88e-02	4.94e-02	2.47e-02	1.24e-02	6.18e-03	3.09e-03
	Order	/	1.00	1.00	1.00	1.00	1.00
	$\lVert u - u_h\rVert_0$	3.95e-03	1.01e-03	2.56e-04	6.43e-05	1.61e-05	4.03e-06
	Order	/	1.97	1.98	1.99	2.00	2.00
	E_C	5.32e-02	2.66e-02	1.33e-02	6.67e-03	3.34e-03	1.67e-03
	Order	/	1.00	1.00	1.00	1.00	1.00
	$E_{\mathcal{V}}$	1.35e-01	6.56e-02	3.24e-02	1.61e-02	8.02e-03	4.00e-03
	Order	/	1.04	1.02	1.01	1.00	1.00
	$E_{\mathcal{M}}$	6.19e-02	3.12e-02	1.57e-02	7.84e-03	3.92e-03	1.96e-03
	Order	/	0.99	1.00	1.00	1.00	1.00

The numerical results are shown in Tables 5 and 6, which are consistent with the theoretical findings of Theorem 4.1, and Corollaries 4.1 and 4.2. One can observe that for Mesh IV, the values of ϱ are negative. That is, there exists one unique finite volume element solution that converges to an exact solution with the desired convergence rates under H^1 and L^2 norms, even though the assumption (**A1**) is not satisfied.

Table 5. Numerical results for Example 5.3 on Meshes I and II.

Mesh	$\#\mathcal{T}_h$	8×8	16×16	32×32	64×64	128×128	256×256
Mesh I	ϱ	6.25e+01	6.25e+01	6.25e+01	6.25e+01	6.25e+01	6.25e+01
	$\lvert u_I - u_h\rvert_1$	4.34e-03	1.30e-03	3.79e-04	1.06e-04	2.87e-05	7.50e-06
	Order	/	1.74	1.78	1.83	1.89	1.93
	$\lvert u - u_h\rvert_1$	2.14e-01	1.07e-01	5.36e-02	2.68e-02	1.34e-02	6.69e-03
	Order	/	1.00	1.00	1.00	1.00	1.00
	$\lVert u - u_h\rVert_0$	1.19e-02	2.97e-03	7.40e-04	1.85e-04	4.62e-05	1.16e-05
	Order	/	2.01	2.00	2.00	2.00	2.00
	E_C	3.74e-03	1.24e-03	3.70e-04	1.05e-04	2.84e-05	7.42e-06
	Order	/	1.59	1.74	1.82	1.89	1.93
	$E_{\mathcal{V}}$	1.26e-02	3.29e-03	8.51e-04	2.19e-04	5.58e-05	1.41e-05
	Order	/	1.94	1.95	1.96	1.97	1.98
	$E_{\mathcal{M}}$	7.94e-03	2.21e-03	5.96e-04	1.58e-04	4.10e-05	1.05e-05
	Order	/	1.85	1.89	1.92	1.94	1.97
Mesh II	ϱ	5.53e+01	6.02e+01	6.19e+01	6.23e+01	6.25e+01	6.25e+01
	$\lvert u_I - u_h\rvert_1$	2.64e-02	9.79e-03	2.92e-03	7.94e-04	2.05e-04	5.19e-05
	Order	/	1.43	1.74	1.88	1.95	1.98
	$\lvert u - u_h\rvert_1$	2.20e-01	1.10e-01	5.49e-02	2.74e-02	1.37e-02	6.85e-03
	Order	/	1.00	1.00	1.00	1.00	1.00
	$\lVert u - u_h\rVert_0$	1.26e-02	3.25e-03	8.28e-04	2.08e-04	5.22e-05	1.31e-05
	Order	/	1.95	1.97	1.99	2.00	2.00
	E_C	3.11e-02	1.10e-02	3.20e-03	8.56e-04	2.20e-04	5.56e-05
	Order	/	1.50	1.78	1.90	1.96	1.99
	$E_{\mathcal{V}}$	4.95e-02	1.72e-02	4.87e-03	1.28e-03	3.24e-04	8.15e-05
	Order	/	1.52	1.82	1.93	1.98	1.99
	$E_{\mathcal{M}}$	4.45e-02	1.47e-02	4.13e-03	1.08e-03	2.76e-04	6.95e-05
	Order	/	1.59	1.83	1.93	1.97	1.99

Table 6. Numerical results for Example 5.3 on Meshes III and IV.

Mesh	$\#\mathcal{T}_h$	8×8	16×16	32×32	64×64	128×128	256×256
Mesh III	ϱ	6.18e+01	6.23e+01	6.25e+01	6.25e+01	6.25e+01	6.25e+01
	$\lvert u_I-u_h\rvert_1$	3.83e-03	1.08e-03	2.97e-04	8.00e-05	2.11e-05	5.43e-06
	Order	/	1.83	1.86	1.89	1.93	1.95
	$\lvert u-u_h\rvert_1$	1.75e-01	8.76e-02	4.38e-02	2.19e-02	1.09e-02	5.47e-03
	Order	/	1.00	1.00	1.00	1.00	1.00
	$\lVert u-u_h\rVert_0$	9.07e-03	2.26e-03	5.65e-04	1.41e-04	3.53e-05	8.82e-06
	Order	/	2.00	2.00	2.00	2.00	2.00
	E_C	6.45e-03	1.71e-03	4.49e-04	1.17e-04	3.00e-05	7.63e-06
	Order	/	1.91	1.93	1.94	1.96	1.97
	$E_{\mathcal{V}}$	1.60e-02	4.08e-03	1.03e-03	2.59e-04	6.51e-05	1.63e-05
	Order	/	1.98	1.99	1.99	1.99	1.99
	$E_{\mathcal{M}}$	1.14e-02	2.92e-03	7.44e-04	1.89e-04	4.77e-05	1.20e-05
	Order	/	1.96	1.97	1.98	1.98	1.99
Mesh IV	ϱ	-1.39e+01	-1.39e+01	-1.39e+01	-1.39e+01	-1.39e+01	-1.39e+01
	$\lvert u_I-u_h\rvert_1$	8.71e-03	3.90e-03	1.88e-03	9.29e-04	4.64e-04	2.32e-04
	Order	/	1.16	1.06	1.02	1.00	1.00
	$\lvert u-u_h\rvert_1$	2.29e-01	1.15e-01	5.73e-02	2.87e-02	1.43e-02	7.17e-03
	Order	/	1.00	1.00	1.00	1.00	1.00
	$\lVert u-u_h\rVert_0$	1.33e-02	3.30e-03	8.24e-04	2.06e-04	5.15e-05	1.29e-05
	Order	/	2.01	2.00	2.00	2.00	2.00
	E_C	6.42e-02	3.22e-02	1.61e-02	8.04e-03	4.02e-03	2.01e-03
	Order	/	1.00	1.00	1.00	1.00	1.00
	$E_{\mathcal{V}}$	6.61e-02	3.31e-02	1.66e-02	8.32e-03	4.17e-03	2.08e-03
	Order	/	1.00	1.00	1.00	1.00	1.00
	$E_{\mathcal{M}}$	1.17e-02	4.72e-03	2.14e-03	1.03e-03	5.12e-04	2.55e-04
	Order	/	1.31	1.14	1.05	1.01	1.00

Example 5.4. *Solve Eqs* (2.1) *and* (2.2) *and choose the strongly anisotropic diffusion coefficient and exact solution as follows (see [34]):*

$$\Lambda(x,y)=\frac{1}{x^2+y^2}\begin{pmatrix}\kappa x^2+y^2 & (\kappa-1)xy\\ (\kappa-1)xy & x^2+\kappa y^2\end{pmatrix},\quad u(x,y)=sin(\pi x)sin(\pi y),$$

where κ characterizes the level of anisotropy. The right-hand side function is determined by

$$f(x,y)=\pi^2(1+\kappa)f_1+\frac{\pi(1-\kappa)}{x^2+y^2}(yf_2+xf_3+2\pi xyf_4),$$

with

$$f_1(x,y) = sin(\pi x)sin(\pi y), \qquad f_2(x,y) = sin(\pi x)cos(\pi y),$$
$$f_3(x,y) = cos(\pi x)sin(\pi y), \qquad f_4(x,y) = cos(\pi x)cos(\pi y).$$

In this example, we employ $\kappa = 10^{-3}$.

Note that here, Λ is a variable diffusion coefficient, thus in our numerical experiments, we let Λ be a piecewise constant with respect to $\mathcal{T}_h$, such that $\Lambda_K = \Lambda(\boldsymbol{x}_K)$. Tables 7 and 8 report the numerical results, and we find that the performance is similar to the previous Examples 5.1 and 5.3. Moreover, Examples 5.3 and 5.4 all show that (**A1**) is just a sufficient condition to guarantee coercivity.

Table 7. Numerical results for Example 5.4 on Meshes I and II.

Mesh	$\#\mathcal{T}_h$	8×8	16×16	32×32	64×64	128×128	256×256
Mesh I	ϱ	6.25e-05	6.25e-05	6.25e-05	6.25e-05	6.25e-05	6.25e-05
	$\lvert u_I - u_h\rvert_1$	6.53e-02	1.75e-02	4.65e-03	1.22e-03	3.19e-04	8.25e-05
	Order	/	1.90	1.91	1.93	1.94	1.95
	$\lvert u - u_h\rvert_1$	2.58e-01	1.27e-01	6.31e-02	3.15e-02	1.57e-02	7.87e-03
	Order	/	1.02	1.01	1.00	1.00	1.00
	$\lVert u - u_h\rVert_0$	8.04e-03	2.10e-03	5.41e-04	1.37e-04	3.46e-05	8.67e-06
	Order	/	1.94	1.96	1.98	1.99	2.00
	E_C	5.59e-02	1.57e-02	4.27e-03	1.14e-03	2.99e-04	7.78e-05
	Order	/	1.83	1.88	1.91	1.93	1.94
	$E_{\mathcal{V}}$	1.11e-01	2.94e-02	7.61e-03	1.95e-03	4.97e-04	1.26e-04
	Order	/	1.92	1.95	1.96	1.97	1.98
	$E_{\mathcal{M}}$	7.70e-02	2.08e-02	5.48e-03	1.43e-03	3.70e-04	9.49e-05
	Order	/	1.89	1.92	1.94	1.95	1.96
Mesh II	ϱ	1.30e-05	4.54e-05	5.79e-05	6.13e-05	6.22e-05	6.24e-05
	$\lvert u_I - u_h\rvert_1$	8.29e-02	3.04e-02	1.01e-02	2.93e-03	7.83e-04	2.01e-04
	Order	/	1.45	1.59	1.78	1.90	1.96
	$\lvert u - u_h\rvert_1$	2.71e-01	1.34e-01	6.61e-02	3.28e-02	1.64e-02	8.18e-03
	Order	/	1.02	1.02	1.01	1.00	1.00
	$\lVert u - u_h\rVert_0$	1.07e-02	3.47e-03	1.02e-03	2.77e-04	7.14e-05	1.80e-05
	Order	/	1.63	1.76	1.89	1.96	1.99
	E_C	8.36e-02	3.17e-02	1.04e-02	2.99e-03	7.95e-04	2.03e-04
	Order	/	1.40	1.61	1.80	1.91	1.97
	$E_{\mathcal{V}}$	1.45e-01	4.87e-02	1.46e-02	3.99e-03	1.04e-03	2.62e-04
	Order	/	1.57	1.74	1.87	1.95	1.98
	$E_{\mathcal{M}}$	1.10e-01	3.91e-02	1.22e-02	3.42e-03	8.98e-04	2.28e-04
	Order	/	1.50	1.68	1.84	1.93	1.97

Table 8. Numerical results for Example 5.4 on Meshes III and IV.

Mesh	$\#\mathcal{T}_h$	8×8	16×16	32×32	64×64	128×128	256×256
	ϱ	5.77e-05	6.13e-05	6.22e-05	6.24e-05	6.25e-05	6.25e-05
	$\lvert u_I-u_h\rvert_1$	4.48e-02	1.16e-02	3.00e-03	7.75e-04	2.00e-04	5.12e-05
	Order	/	1.95	1.95	1.95	1.96	1.96
	$\lvert u-u_h\rvert_1$	2.34e-01	1.16e-01	5.78e-02	2.89e-02	1.44e-02	7.22e-03
	Order	/	1.01	1.00	1.00	1.00	1.00
Mesh III	$\lVert u-u_h\rVert_0$	7.18e-03	1.79e-03	4.49e-04	1.12e-04	2.81e-05	7.03e-06
	Order	/	2.00	2.00	2.00	2.00	2.00
	E_C	4.25e-02	1.13e-02	2.98e-03	7.74e-04	2.00e-04	5.15e-05
	Order	/	1.91	1.93	1.94	1.95	1.96
	$E_{\mathcal{V}}$	9.23e-02	2.42e-02	6.17e-03	1.57e-03	3.96e-04	9.98e-05
	Order	/	1.93	1.97	1.98	1.98	1.99
	$E_{\mathcal{M}}$	6.42e-02	1.68e-02	4.33e-03	1.11e-03	2.82e-04	7.16e-05
	Order	/	1.93	1.96	1.97	1.97	1.98
	ϱ	-3.87e-04	-4.05e-04	-4.05e-04	-4.05e-04	-4.05e-04	-4.05e-04
	$\lvert u_I-u_h\rvert_1$	7.72e-02	2.66e-02	1.17e-02	5.77e-03	2.85e-03	1.39e-03
	Order	/	1.53	1.18	1.02	1.02	1.04
	$\lvert u-u_h\rvert_1$	3.01e-01	1.49e-01	7.43e-02	3.72e-02	1.86e-02	9.28e-03
	Order	/	1.01	1.00	1.00	1.00	1.00
Mesh IV	$\lVert u-u_h\rVert_0$	1.07e-02	2.85e-03	7.41e-04	1.88e-04	4.74e-05	1.19e-05
	Order	/	1.90	1.94	1.97	1.99	2.00
	E_C	1.28e-01	6.00e-02	2.96e-02	1.48e-02	7.38e-03	3.68e-03
	Order	/	1.10	1.02	1.00	1.00	1.01
	$E_{\mathcal{V}}$	2.33e-01	1.17e-01	5.82e-02	2.90e-02	1.45e-02	7.24e-03
	Order	/	1.00	1.00	1.00	1.00	1.00
	$E_{\mathcal{M}}$	1.29e-01	5.88e-02	2.87e-02	1.43e-02	7.12e-03	3.55e-03
	Order	/	1.14	1.04	1.01	1.00	1.00

6. Conclusions

We improved the coercivity and established the superconvergence of the isoparametric bilinear finite volume element scheme that was constructed in [17]; namely, the scheme is obtained by using the trapezoidal rule to approximate the line integrals in classical Q_1-FVEM. A new sufficient condition is proposed to guarantee the coercivity result of this scheme, which improved the coercivity result in [17]; see Theorem 3.2. We mention that the weaker condition (**A1**) is a basis for various error estimates. Assume that the quadrilateral mesh is h^2-uniform, and we reach the superconvergence property $|u_I -$

$u_h|_1 = O(h^2)$. As a by-product, we prove that u_h converges to u with optimal convergence order 1 (resp. 2) under H^1 (resp. L^2) norm. Moreover, the superconvergence results of u_h at geometric centers, interior vertices, and edge midpoints are also obtained in an average gradient norm. The numerical results in Examples 5.3 and 5.4 imply that, there exists one unique finite volume element solution that converges to the exact solution with the desired convergence orders under H^1 and L^2 norms, even though (**A1**) is violated. In summary, (**A1**) is just a sufficient condition to guarantee coercivity.

To obtain the superconvergence result, previous works required a strong mesh condition, e.g., rectangular mesh or h^2-uniform quadrilateral mesh [4, 27, 30, 31, 46]. Thus, the weakening of h^2-uniform quadrilateral mesh condition is not easy. Moreover, if we slightly violate the h^2-uniform quadrilateral mesh (e.g., Mesh IV, uniform trapezoidal mesh in Section 5), the superconvergence result is not valid. In the future, we expect that the presented analysis can be applied to biquadratic finite volume element schemes over quadrilateral meshes. For this purpose, there are some difficulties that need to be overcome. First, how to appropriately express the 9×9 element stiffness matrix. Second, the spectral analysis of element stiffness matrix is not easy, and how to derive a sufficient condition (with analytic expression) to guarantee the coercivity remains unknown. Third, to establish the superconvergence, the difference between finite element and finite volume element bilinear forms needs to be carefully investigated.

Author contributions

Shengying Mu: Formal analysis, investigation, software, writing - original draft; Yanhui Zhou: Conceptualization, funding acquisition, writing - review and editing, supervision. All authors have read and approved the final version of the manuscript for publication.

Use of Generative-AI tools declaration

The authors declare they have not used Artificial Intelligence (AI) tools in the creation of this article.

Acknowledgments

The authors would like to thank the reviewers for the carefully readings and providing some insightful comments and suggestions, that lead to an improvement of the presentation. This work was supported by the National Natural Science Foundation of China (No. 12401517), NSF of Guangdong Province (No. 2023A1515010885) and the project of promoting research capabilities for key constructed disciplines in Guangdong Province (No. 2021ZDJS028).

Conflict of interest

The authors declared that they have no conflicts of interest regarding the publication of this work.

References

1. R. E. Bank, D. J. Rose, Some error estimates for the box method, *SIAM J. Numer. Anal.*, **24** (1987), 777–787.

2. Z. Cai, On the finite volume element method, *Numer. Math.*, **58** (1990), 713–735. https://doi.org/10.1007/BF01385651

3. J. S. Camier, F. Hermeline, A monotone nonlinear finite volume method for approximating diffusion operators on general meshes, *Int. J. Numer. Meth. Engng.*, **107** (2016), 496–519. https://doi.org/10.1002/nme.5184

4. W. Cao, Z. Zhang, Q. Zou, Is 2k-Conjecture valid for finite volume methods? *SIAM J. Numer. Anal.*, **53** (2015), 942–962.

5. G. Chen, J. Lv, X. Zhang, Finite volume element method for nonlinear elliptic equations on quadrilateral meshes, *Comput. Math. Appl.*, **140** (2023), 154–168. https://doi.org/10.1016/j.camwa.2023.04.010

6. Z. Chen, J. Wu, Y. Xu, Higher-order finite volume methods for elliptic boundary value problems, *Adv. Comput. Math.*, **37** (2012), 191–253. https://doi.org/10.1007/s10444-011-9201-8

7. S. Chou, S. He, On the regularity and uniformness conditions on quadrilateral grids, *Comput. Methods Appl. Mech. Engrg.*, **191** (2002), 5149–5158. https://doi.org/10.1016/S0045-7825(02)00357-2

8. S. Chou, X. Ye, Superconvergence of finite volume methods for the second order elliptic problem, *Comput. Methods Appl. Mech. Eng.*, **196** (2007), 3706–3712. https://doi.org/10.1016/j.cma.2006.10.025

9. X. Dai, Z. Yang, A. Zhou, Symmetric finite volume schemes for eigenvalue problems in arbitrary dimensions, *Sci. China Ser. A-Math.*, **51** (2008), 1401–1414. https://doi.org/10.1007/s11425-008-0102-3

10. C. Erath, D. Praetorius, Adaptive vertex-centered finite volume methods for general second-order linear elliptic partial differential equations, *IMA J. Numer. Anal.*, **39** (2019), 983–1008. https://doi.org/10.1093/imanum/dry006

11. R. E. Ewing, T. Lin, Y. Lin, On the accuracy of the finite volume element method based on piecewise linear polynomials, *SIAM J. Numer. Anal.*, **39** (2002), 1865–1888.

12. R. E. Ewing, M. M. Liu, J. Wang, Superconvergence of mixed finite element approximations over quadrilaterals, *SIAM J. Numer. Anal.*, **36** (1999), 772–787. https://doi.org/10.1137/S0036142997322801

13. F. Fang, Q. Hong, J. Wu, Analysis of a special Q_1-finite volume element scheme for anisotropic diffusion problems, *Numer. Math. Theor. Meth. Appl.*, **12** (2019), 1141–1167. https://doi.org/10.4208/nmtma.OA-2018-0080

14. Z. Fang, J. Zhao, H. Li, Y. Liu, Finite volume element methods for two-dimensional time fractional reaction-diffusion equations on triangular grids, *Appl. Anal.*, **102** (2023), 2248–2270. https://doi.org/10.1080/00036811.2022.2027374

15. W. Hackbusch, On first and second order box schemes, *Computing*, **41** (1989), 277–296. https://doi.org/10.1007/BF02241218

16. W. He, Z. Zhang, Q. Zou, Maximum-norms error estimates for high-order finite volume schemes over quadrilateral meshes, *Numer. Math.*, **138** (2018), 473–500. https://doi.org/10.1007/s00211-017-0912-8

17. Q. Hong, J. Wu, Coercivity results of a modified Q_1-finite volume element scheme for anisotropic diffusion problems, *Adv. Comput. Math.*, **44** (2018), 897–922. https://doi.org/10.1007/s10444-017-9567-3

18. Q. Hong, J. Wu, A Q_1-finite volume element scheme for anisotropic diffusion problems on general convex quadrilateral mesh, *J. Comput. Appl. Math.*, **372** (2020), 112732. https://doi.org/10.1016/j.cam.2020.112732

19. S. Karaa, K. Mustapha, A. K. Pani, Finite volume element method for two-dimensional fractional subdiffusion problems, *IMA J. Numer. Anal.*, **37** (2017), 945–964. https://doi.org/10.1093/imanum/drw010

20. P. Lesaint, M. Zlámal, Superconvergence of the gradient of finite element solutions, *RAIRO Anal. Numér.*, **13** (1979), 139–166.

21. R. Li, Z. Chen, W. Wu, Generalized difference methods for differential equations: Numerical analysis of finite volume methods, Boca Raton: CRC Press, 2000. https://doi.org/10.1201/9781482270211

22. R. Li, P. Zhu, Generalized difference methods for second order elliptic partial differential equations (I)-triangle grids, (in chinese), *Numer. Math. J. Chin. Univ.*, **16** (1982), 140–152. https://doi.org/10.1016/0898-1221(88)90144-7

23. Y. Li, R. Li, Generalized difference methods on arbitrary quadrilateral networks, *J. Comput. Math.*, **17** (1999), 653–672.

24. Y. Lin, J. Liu, M. Yang, Finite volume element methods: An overview on recent developments, *Int. J. Numer. Anal. Model.*, **4** (2013), 14–34.

25. Y. Lin, M. Yang, Q. Zou, L^2 error estimates for a class of any order finite volume schemes over quadrilateral meshes, *SIAM J. Numer. Anal.*, **53** (2015), 2030–2050. https://doi.org/10.1137/140963121

26. Y. Lou, X. Guo, H. Rui, X. Feng, Quadratic discontinuous finite volume element schemes for Stokes-Darcy problems, *J. Comput. Phys.*, **530** (2025), 113898. https://doi.org/10.1016/j.jcp.2025.113898

27. J. Lv, Y. Li, L^2 error estimates and superconvergence of the finite volume element methods on quadrilateral meshes, *Adv. Comput. Math.*, **37** (2012), 393–416. https://doi.org/10.1007/s10444-011-9215-2

28. S. Mu, Y. Zhou, An analysis of the isoparametric bilinear finite volume element method by applying the Simpson rule to quadrilateral meshes, *AIMS Mathematics*, **8** (2023), 22507–22537. https://doi.org/10.3934/math.20231147

29. C. Nie, J. Fang, S. Shu, A monotone finite volume element scheme for diffusion equations on arbitrary polygonal grids, *Comput. Math. Appl.*, **153** (2024), 225–236. https://doi.org/10.1016/j.camwa.2023.11.030

30. S. Shu, H. Yu, Y. Huang, C. Nie, A symmetric finite volume element scheme on quadrilateral grids and superconvergence, *Int. J. Numer. Anal. Mod.*, **3** (2006), 348–360.

31. T. Wang, Y. Gu, Superconvergent biquadratic finite volume element method for two-dimensional Poisson's equations, *J. Comput. Appl. Math.*, **234** (2010), 447–460.

32. X. Wang, Y. Li, L^2 error estimates for high order finite volume methods on triangular meshes, *SIAM J. Numer. Anal.*, **54** (2016), 2729–2749.

33. X. Wang, Y. Zhang, Z. Zhang, Flexible ultra-convergence structures for the finite volume element method, *J. Sci. Comput.*, **101** (2024), 15. https://doi.org/10.1007/s10915-024-02654-7

34. J. Wu, Z. Gao, Z. Dai, A vertex-centered linearity-preserving discretization of diffusion problems on polygonal meshes, *Internat. J. Numer. Methods Fluids*, **81** (2016), 131–150. https://doi.org/10.1002/fld.4178

35. J. Xu, Q. Zou, Analysis of linear and quadratic simplicial finite volume methods for elliptic equations, *Numer. Math.*, **111** (2009), 469–492. https://doi.org/10.1007/s00211-008-0189-z

36. W. Xu, L. Ge, Two-grid finite volume element methods for solving Cahn-Hilliard equation, *Bull. Iran. Math. Soc.*, **49** (2023), 28. https://doi.org/10.1007/s41980-023-00774-8

37. J. Zhang, Z. Chen, L^2 error estimates for a family of cubic finite volume methods on triangular meshes, *Comput. Math. Appl.*, **143** (2023), 189–223. https://doi.org/10.1016/j.camwa.2023.04.038

38. J. Zhang, Tetrahedral quadratic finite volume method schemes for the Stokes equation, *J. Comput. Appl. Math.*, **463** (2025), 116472. https://doi.org/10.1016/j.cam.2024.116472

39. L. Zhang, L. Li, On superconvergence of isoparametric bilinear finite elements, *Comm. Numer. Methods Engrg.*, **12** (1996), 849–862.

40. Y. Zhang, A quadratic serendipity finite volume element method on arbitrary convex polygonal meshes, *Commun. Comput. Phys.*, **34** (2023), 116–131. https://doi.org/10.4208/cicp.OA-2022-0307

41. Y. Zhang, J. Wu, An adaptive polygonal finite volume element method based on the mean value coordinates for anisotropic diffusion problems, *Commun. Comput. Phys.*, **37** (2025), 783–809. https://doi.org/10.4208/cicp.OA-2023-0213

42. Y. Zhang, X. Wang, Unified construction and L^2 analysis for the finite volume element method over tensorial meshes, *Adv. Comput. Math.*, **49** (2023), 2. https://doi.org/10.1007/s10444-022-10004-0

43. Y. Zhang, C. Chen, C. Bi, A quadratic finite volume method for nonlinear elliptic problems, *Adv. Comput. Math.*, **47** (2021), 32. https://doi.org/10.1007/s10444-021-09853-y

44. Z. Zhang, Q. Zou, Some recent advances on vertex centered finite volume element methods for elliptic equations, *Sci. China Math.*, **56** (2013), 2507–2522. https://doi.org/10.1007/s11425-013-4740-8

45. Z. Zhang, Q. Zou, Vertex-centered finite volume schemes of any order over quadrilateral meshes for elliptic boundary value problems, *Numer. Math.*, **130** (2015), 363–393. https://doi.org/10.1007/s00211-014-0664-7

46. Y. Zhou, Stability and superconvergence of a special Q_1-finite volume element scheme over quadrilateral meshes, *Int. J. Numer. Anal. Mod.*, **22** (2025), 556–584. https://doi.org/10.4208/ijnam2025-1024

47. Y. Zhou, S. Su, A novel family of Q_1-finite volume element schemes on quadrilateral meshes, *Comput. Math. Appl.*, **172** (2024), 216–240. https://doi.org/10.1016/j.camwa.2024.08.019

48. Y. Zhou, J. Wu, A unified analysis of a class of quadratic finite volume element schemes on triangular meshes, *Adv. Comput. Math.*, **46** (2020), 71. https://doi.org/10.1007/s10444-020-09809-8

49. Y. Zhou, Y. Zhang, J. Wu, A polygonal finite volume element method for anisotropic diffusion problems, *Comput. Math. Appl.*, **140** (2023), 225–236. https://doi.org/10.1016/j.camwa.2023.04.025

50. Q. D. Zhu, Q. Lin, *Superconvergence theory of the finite element method*, (in Chinese), Hunan: Hunan Science Press, 1989.

51. Q. Zou, An unconditionally stable quadratic finite volume scheme over triangular meshes for elliptic equations, *J. Sci. Comput.*, **70** (2017), 112–124. https://doi.org/10.1007/s10915-016-0244-3

AIMS Press